

The manuscript has been accepted for publication:

Zhao, W., Singh, K. and Kapania, R. K., "Thermal Buckling Analysis and Optimization of Curvilinearly Stiffened Plates with Variable Angle Tow Laminates," AIAA Journal of Spacecraft and Rockets, 2018, DOI: 10.2514/1.A34378 (<http://arc.aiaa.org/doi/abs/10.2514/1.A34378>)

Thermal Buckling Analysis and Optimization of Curvilinearly Stiffened Plates with Variable Angle Tow Laminates

Wei Zhao*, Karanpreet Singh† and Rakesh K. Kapania‡

Virginia Polytechnic Institute and State University, Blacksburg, VA, 24061

This paper presents results from thermal buckling analysis and optimization of stiffened composite panels with variable angle tow laminates and curvilinear stiffeners. Considering the meshing difficulties for curvilinearly stiffened variable angle tow laminates due to both spatially dependent fiber path orientation and arbitrarily shaped stiffeners in the traditional finite element analysis, the present work models the plate and stiffeners separately without the need to place finite element nodes along the stiffener/plate and stiffener/stiffener interfaces. The displacement compatibility conditions are enforced at these interfaces in the finite element analysis. Convergence and verification study results show that the present method can accurately predict the thermal buckling behaviors of variable angle tow laminates and curvilinearly stiffened variable angle tow laminates. Parametric studies show that either variable angle tow laminates or curvilinear stiffeners alone can improve the buckling performance as compared to using straight fiber laminates and straight stiffeners. Variable angle tow laminates and curvilinear stiffeners are found to redistribute the in-plane stress resultants and tailor the buckling mode shape, respectively, to improve the total buckling response. Optimization studies using curvilinear stiffeners and variable angle tow laminates together for maximizing buckling temperature for a stiffened plate are conducted.

*Post-doctoral Fellow, Kevin T. Crofton Department of Aerospace and Ocean Engineering, AIAA Member, weizhao@vt.edu

†Graduate Research Assistant, Kevin T. Crofton Department of Aerospace and Ocean Engineering, AIAA Student Member, kasingh@vt.edu

‡Norris and Wendy Mitchell Endowed Professor, Kevin T. Crofton Department of Aerospace and Ocean Engineering, AIAA Associate Fellow, rkapania@vt.edu

Nomenclature

A_s	stiffener cross-sectional area, m ²
a	length of the composite panel, m
\mathbf{B}	strain-displacement relation matrix
b	width of the composite panel, m
b_s	width of the composite stiffener, m
\mathbf{D}	constitutive matrix giving stress resultant-strain relations
d_p	panel displacement, m
d_s	stiffener displacement described in the local coordinate system, m
d_{sg}	stiffener displacement described in the global coordinate system, m
e	eccentricity of the stiffener, $e = \frac{1}{2} (t_p + h_s)$, m
h_s	stiffener height, m
\mathbf{J}	Jacobian of the coordinate transformation
\mathbf{K}_p	panel elastic stiffness matrix
\mathbf{K}_s	stiffener elastic stiffness matrix
\mathbf{K}_{Gp}	panel geometric stiffness matrix
\mathbf{K}_{Gs}	stiffener geometric stiffness matrix
\mathbf{N}_{sp}	shape functions to represent stiffener nodal displacement using panel nodal displacement
N_{XX}, N_{YY}, N_{XY}	in-plane stress resultants, N/mm
\mathbf{T}_s	transformation matrix
t_p	panel thickness, m
W_s	stiffeners structural weight, kg
$W_{s,0}$	structural weight for two straight x -axis stiffeners, kg
W_t	total structural weight for the stiffened plate, kg
Γ	stiffener arch length domain
Ω	panel area domain
ξ, η	natural coordinates
ε, σ	strain and stress (Pa), respectively
$\boldsymbol{\sigma}$	stress matrix for computing geometric stiffness
λ_b	buckling load factor

$\Delta\varepsilon$	parameter for the stiffener placement
ΔT	temperature gradient, °C
θ	variable fiber ply angle, degrees
$\Theta_{1,2}$	variable fiber ply angles at plate's center, $\bar{x} = 0$ and edge, $ \bar{x} = 1$, respectively, degrees
$(\cdot)_{cr}$	critical buckling
$(\cdot)_p$	expression for the plate
$(\cdot)_s$	expression for the stiffener
$(\cdot)^T$	transpose operator
$(\cdot)_T$	thermal response

I. Introduction

High-speed launch and re-entry vehicles are subjected to severe environments during their normal operations, such as aerodynamic heating. The importance of thermal effects on high-speed air vehicle design has received attention as early as during the World War II [1]. Both material degradation in high temperature and thermal stresses due to restrained thermal expansions generated at an elevated temperature may cause a structure failure and reduce both the safety and the life of a supersonic and hypersonic vehicle.

Composite structures have been widely used in spacecraft launch vehicles and re-entry vehicles due to their higher strength-to-weight ratio [2, 3] and higher heat resistant properties [4]. The innovative technologies for composites manufacturing, such as, Automated Fiber Placement (AFP) [5] have made it possible to fabricate spatially-varying angle fiber-ply laminate for composites to further improve the structural performances [6]. Additionally, the fabrication technologies for integrally stiffened panels, such as using Vacuum Assisted Resin Transfer Molding (VARTM) and Pi-Joining as summarized in Ref. [7] and the Pultruded Rod Stitched Efficient Unitized Structure (PRSEUS) concept using the stitched-composite technology [8], leads to a further improvement in the structural performance. The development in the manufacturing technologies along with the super/hypersonic flight induced thermal effects for the high speed vehicle local panels lead to an interest in studying the structural performance of stiffened panels with both variable angle tow (VAT) laminates and arbitrarily shaped stiffeners in the presence of the thermal loads.

For local panels used in a hypersonic vehicle, thermal loads are generated by the temperature change due to the aerodynamic heating and the restrained thermal expansion [9]. This phenomena is common for

restrained panels of high speed launch and re-entry vehicles. Various approaches were studied for performing thermal buckling of composite plates and shells with straight fibers [10–13], and thermal buckling of structures made of functionally graded materials [14, 15]. A recent work on thermal buckling analysis of VAT laminated plate [16] showed that an increased buckling load can be obtained by tailoring the curved fiber path orientation in the panel as compared to that using straight fiber path laminates. IJsselmuiden *et al.* [17] studied thermo-mechanical buckling optimization of VAT laminated panels. They found that the proper tailoring of both the stiffness and thermal properties for a VAT laminated plate can increase the buckling loads significantly as compared to the quasi-isotropic laminated panels. All these works demonstrate the benefits of using VAT laminates to improve the buckling response of such panels under thermal loads.

Static and buckling analyses of VAT laminated panels have received considerable interest during last several decades. Gürdal *et al.* [18] found that the VAT laminates can tailor the in-plane stress resultants to a favorable one that can improve the buckling load. Based on this finding by Gürdal *et al.* [18], several optimization studies on buckling maximization of a VAT laminated plate have been conducted. Setoodeh *et al.* [19] used a finite element method and a gradient-based approach for optimizing fiber path orientations for VAT laminated plates. The optimization results showed a significant improvement in the buckling loads of a VAT laminated plate as compared to a plate with straight fiber path laminates. IJsselmuiden *et al.* [20] conducted a buckling load maximization for VAT laminated panels using a finite element method and lamination parameters. They also found that a significant improvement in the buckling load is observed for a plate by using VAT laminates as compared to that with straight fiber path laminates. These optimization studies [19, 20] found that it is the in-plane load redistribution through tailoring the fiber path orientations that leads to an improvement in the buckling load for the VAT laminated structures. Wu *et al.* [21] used the Rayleigh-Ritz approach for performing the buckling analysis of a VAT laminated plate and a genetic algorithm as the optimizer to perform the buckling load maximization. A nonlinear distribution of fiber ply angles was considered to achieve a maximum buckling load which is close to that obtained using lamination parameters as studied by IJsselmuiden *et al.* [20].

Additionally, stiffeners could be added to further improve the buckling load of VAT laminated plates by modifying the buckling mode wavelength. Coburn *et al.* [22] used the Rayleigh-Ritz method to study both the local and global buckling responses of stiffened VAT laminated plates. Inspired from nature, Kapania, *et al.* [23] found that curvilinear stiffeners are able to improve the buckling loads for the panel under certain loads as compared to that using straight-stiffeners. Zhao and Kapania [24] studied the buckling of curvilinearly stiffened composite plate in the presence of both the in-plane axial and shear loads. The

parametric study results in their work reveal that it is possible to improve the buckling responses in terms of tailoring the stiffener shapes for modifying the buckling mode shape. Our recent work [25] also showed that the capability of the in-plane stress redistribution of using VAT laminates can improve the buckling responses for both unstiffened and stiffened laminated plates. Due to the ability of modifying the buckling mode shape using curvilinear stiffeners and the in-plane stress redistribution of using VAT laminates for a plate, Stanford and Jutte [26] studied the aircraft wing box design using both curvilinear stiffeners and tow-steered composites together for wing panel design. Their results showed that an integrated design leads to a larger weight reduction as compared to the design of using them independently. Singh and Kapania [27] studied buckling maximization for a composite panel with both curvilinear fibers and curvilinear stiffeners. Their research showed a substantial benefit of using the two technologies simultaneously for maximizing the panel buckling loads. These two representative optimization results [26, 27] drive the research interest to study the buckling response of the VAT laminated plate with curvilinear stiffeners in the presence of thermal loads. Considering the manufacturing constraints of fabricating the laminated stiffeners that cross each other, without a loss of generality, the stiffener is modeled as an orthotropic beam.

For studying the structural responses of the stiffened VAT laminates with arbitrarily shaped stiffeners, both spatially dependent fiber ply orientation and arbitrarily shaped stiffeners could lead to difficulties for generating a mesh or obtaining a converged mesh for such structures when using a finite element analysis. A previously developed curvilinearly stiffened panel design optimization framework, EBF3PanelOpt [28] by Mulani, *et al.*, used a commercially available FEA package, MSC PATRAN, to mesh such structures, which requires placing nodes at the stiffener/plate and stiffener/stiffener interfaces. An increase in the stiffener number increases the number of design variables and the difficulty in meshing such structures with many arbitrarily shaped stiffeners, it was recommended to use a maximum of six stiffeners in shape optimization when using EBF3PanelOpt [28].

One useful approach of studying the influence of stiffener shape on panel's buckling response is the smeared stiffness approach [29–32]. This approach mimics the laminate fibers by formulating the stiffeners stiffness in terms of *ABD* matrix for the plate, which simplifies the modeling process and increases the analysis speed without remeshing the plate when there is a change in the stiffener shape. The superposition principle is used for the stiffened plate's stiffness by adding stiffness terms for the plate and stiffeners. This method enables the use of gradient based optimization for maximizing the buckling loads in terms of stiffeners shape [33]. However, this method is limited to the grid-stiffened structures, which means that stiffeners number, placement and shape for structures should be similar to laminate fibers. Considering the method presented

in the paper works for arbitrary number and arbitrarily shaped stiffeners for the plate, the smeared stiffness approach could limit the design space of stiffeners for improving the buckling load.

An emerging technology developed in MSC PATRAN/NASTRAN, named glue contact [34], which is an automated technique that can be used to merge two surfaces together using multipoint constraints. This technology releases the constraint in placing nodes at the stiffener/plate interfaces when meshing the curvilinearly stiffened structures for a finite element analysis. Levia [35] used this technology to study the effect of curvilinear spars and ribs in aircraft wing box design to avoid a repeated meshing work during shape optimization. Singh and Kapania [36] used this technology for studying the mechanical buckling optimization of curvilinearly stiffened plates with VAT laminates. However, the optimization problem becomes complex during the automatic pre-processing for such structures with many arbitrarily shaped stiffeners because the common nodes at the stiffener/stiffener interfaces still should be considered. The number and shape of curvilinear stiffeners increase the difficulty in meshing such structures for performing finite element analysis even when using the glue contact.

Additionally, glue contact is very sensitive to the offsets and gaps between the two models that are to be joined together. Along with some other limitations, such as those pointed out by Ahlbert [37], the glue contact could affect the accuracy of the analysis results or limit the design space in optimizing the stiffener shape for a stiffened structure. In view of these limitations of glue contact technique for conducting shape optimization of curvilinearly stiffened plates, this paper uses an attractive, efficient finite element approach developed by Zhao and Kapania [24, 25] for studying the buckling responses of a stiffened VAT laminated plate with arbitrarily shaped stiffeners. The present approach obviates the need for placing nodes at both the stiffener/plate and stiffener/stiffener interfaces, which avoids a repeated meshing of the stiffened plate in the shape optimization for determining the optimal stiffener shape. The finite element method is used here so that the developed method can compute the objective function and the constraints for use in any stiffened panel design optimization framework, e.g., EBF3PanelOpt [28]. On the other hand, the finite element method works for any shaped panel with any sets of boundary conditions. Additionally, the present method integrates the stiffness matrix for the VAT laminated panel, wherein the fiber ply orientation for each layer is evaluated for each element.

The primary focus of this paper is to present buckling analysis method for a stiffened plate with both VAT laminates and arbitrarily shaped stiffeners in the presence of thermal loads. After that, structural optimization is conducted in terms of VAT laminates fiber ply orientations and stiffener shape by using the present structural analysis approach for a thermal buckling temperature maximization study. The

paper is organized as follows: Section II derives the elastic stiffness and geometric stiffness matrices for the curvilinearly stiffened VAT laminated plate considering the thermal effect, and presents the approximation of the stiffener displacement in terms of the panel's displacement for transforming the stiffeners' elastic and geometric stiffness to those for the panel. Section III presents a geometry parameterization for an arbitrarily shaped stiffener using Hobby spline [38]. Convergence and verification studies regarding the thermal buckling for composite plates with both straight fiber and VAT laminates are conducted in Section IV. Section V presents verifications on thermal buckling of curvilinearly stiffened, VAT laminated plates and conducts parametric and optimization studies on thermal buckling of stiffened plates with both VAT laminates and arbitrarily shaped stiffeners. The last section, VI, presents concluding remarks.

II. Formulations

A. Thermo-elastic Analysis of Stiffened VAT Laminates

Consider a curvilinearly stiffened panel as shown in Fig. 1a. The panel middle plane Oxy is chosen as the reference plane of the global coordinate system. The composite panel has length, width and thickness denoted as a , b and t_p , respectively. The first-order shear deformation displacement is considered for modeling the plate based on the Mindlin plate theory. Linearly distributed temperature can be considered along the thickness direction for the stiffened panel as shown in Fig. 1b. For the temperature gradient along the laminated panel thickness, normally the temperature decreases from the bottom side to the upper side as shown in Fig. 1b. It is assumed that the temperature gradient varies from ΔT_b to ΔT_m in the panel and from ΔT_m to ΔT_u in the stiffener. When $\Delta T_b = \Delta T_m = \Delta T_u$, a uniform temperature gradient is obtained in the structure. In the present work, the degradation of material properties with temperature is not considered. This assumption is equivalent to a study for the plate in a steady temperature distribution state.

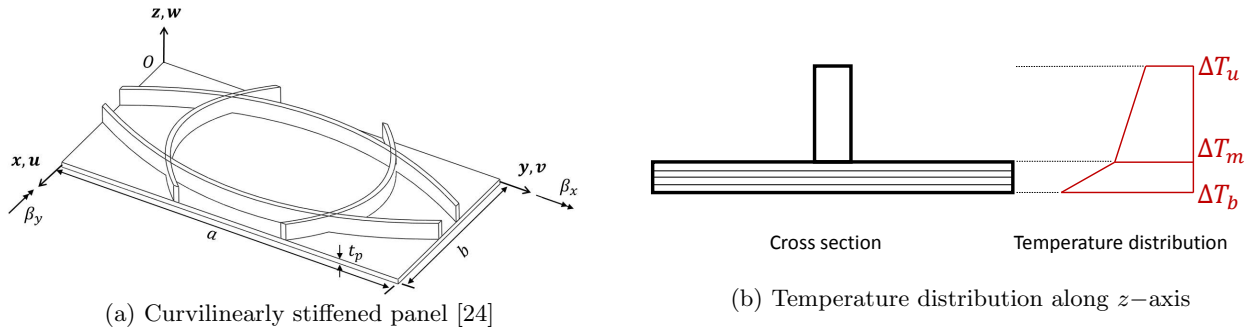


Figure 1: Curvilinearly stiffened panel and temperature distribution

1. Variable angle tow (VAT) laminated plate

For the VAT laminates, there are several parameterizations available to describe the spatially dependent fiber ply orientations, such as linear variation based flow path [6], the Lagrange polynomials method based nonlinear fiber orientations [21] and B-spline based expression [39]. Considering that the scope of the present paper is to study the effect of VAT laminates and curvilinear stiffeners on the structural's buckling responses, for simplicity, a linear, 1-D variation of a reference fiber path is considered. This linear variation along the panel length direction, *i.e.*, x -axis, can be given as [6]:

$$\theta(x) = 2(\Theta_1 - \Theta_0)|\frac{x}{a}| + \Theta_0 = (\Theta_1 - \Theta_0)|\bar{x}| + \Theta_0 \quad (1)$$

where Θ_0 and Θ_1 are fiber ply orientations at two prescribed locations, $\bar{x} = 0$ and $|\bar{x}| = 1$, respectively. The variation of the fiber ply orientation is assumed to be linear and \bar{x} is a normalized length used in the natural coordinate system ranging from -1 to 1. The laminate configuration for the VAT laminates is characterised as $[(\Theta_0 | \Theta_1)_k]_{AS}$ where k is the number of layers and *AS* means an antisymmetric laminate.

Note that the thermal stresses are not caused by external loads but the restrained thermal expansions. The resultant stress-strain relation for each layer for each element described in the global coordinate system, say k^{th} layer [40, 41], is:

$$\begin{Bmatrix} \sigma_x \\ \sigma_y \\ \tau_{xy} \end{Bmatrix}^k = \begin{bmatrix} \bar{Q}_{11}[\theta(\bar{x})] & \bar{Q}_{12}[\theta(\bar{x})] & \bar{Q}_{16}[\theta(\bar{x})] \\ \bar{Q}_{12}[\theta(\bar{x})] & \bar{Q}_{22}[\theta(\bar{x})] & \bar{Q}_{26}[\theta(\bar{x})] \\ \bar{Q}_{16}[\theta(\bar{x})] & \bar{Q}_{26}[\theta(\bar{x})] & \bar{Q}_{66}[\theta(\bar{x})] \end{bmatrix}^k \begin{Bmatrix} \varepsilon_x - \alpha_x[\theta(\bar{x})]\Delta T(z) \\ \varepsilon_y - \alpha_y[\theta(\bar{x})]\Delta T(z) \\ \gamma_{xy} - \alpha_{xy}[\theta(\bar{x})]\Delta T(z) \end{Bmatrix}^k \quad (2)$$

where α_x , α_y and α_{xy} are thermal expansion coefficients described in the global coordinate system. ΔT is the temperature gradient at a certain point along the z -axis with respect to the stress-free state. For the panel, the temperature change is assumed to be $\Delta T = \Delta T_b + k_1 \times z$. When $k_1 = 0$, a uniform temperature change along the panel thickness direction can be obtained.

Equation (2) can be re-written as a matrix format:

$$\boldsymbol{\sigma}_p = \bar{\boldsymbol{Q}}(\boldsymbol{\varepsilon}_p - \boldsymbol{\varepsilon}_{p,T}) \quad (3)$$

where $\boldsymbol{\varepsilon}_{p,T}$ and $\boldsymbol{\varepsilon}_p$ are, respectively, thermal strain vector and elastic strain vector, and $\bar{\boldsymbol{Q}}$ is the reduced stiffness matrix for composite [42].

The total potential energy for the plate for thermo-elastic analysis is

$$\Pi_p = \frac{1}{2} \iiint_V \boldsymbol{\sigma}_p^T (\boldsymbol{\varepsilon}_p - \boldsymbol{\varepsilon}_{p,T}) dV = \frac{1}{2} \iiint_V \left(\mathbf{d}_p^T \mathbf{B}^T \bar{\mathbf{Q}}^T \mathbf{B} \mathbf{d}_p - 2 \mathbf{d}_p^T \mathbf{B}^T \bar{\mathbf{Q}}^T \boldsymbol{\varepsilon}_{p,T} + \boldsymbol{\varepsilon}_{p,T}^T \bar{\mathbf{Q}}^T \boldsymbol{\varepsilon}_{p,T} \right) dV \quad (4)$$

2. Composite Curved Stiffeners

Consider a curved blade stiffener as shown in Fig. 2. The stiffener is modeled using composite beam elements, based on Timoshenko beam theory. The stiffener shape is arbitrary, curvilinear. The solid rectangular cross section of the stiffener has width and height denoted as b_s and h_s , respectively. The stiffener eccentricity, e , is defined as a measure of the offset between the stiffener neutral line and the panel middle plane, $e = \frac{1}{2} (h_s + t_p)$. When the stiffener neutral line coincides with the panel middle plane, $e = 0$, we called the plate as a concentrically stiffened panel. The warping of the stiffener is ignored in this study because the stiffener motion is governed by the plate. A local curvilinear coordinate system $t n b$ is used to describe the motion of the curved stiffener shown in Fig. 2.

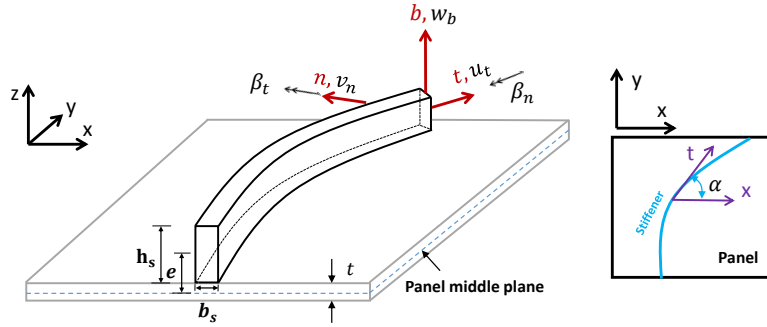


Figure 2: Definitions of displacement and local coordinate system for curved stiffeners [24]

Because the stiffener's start and end points are located in the panel's edges, the stiffener is only restrained in its tangential direction, t -axis, and the other directions are free. Hence, the thermal strain along the principal direction, 1 -axis, is considered. The stress-strain relation for an orthotropic stiffener is given as:

$$\begin{Bmatrix} \sigma_{tt} \\ \sigma_{nn} \\ \sigma_{bb} \\ \tau_{nb} \\ \tau_{tb} \\ \tau_{tn} \end{Bmatrix} = \begin{bmatrix} C_{11} & C_{12} & C_{13} & 0 & 0 & 0 \\ C_{12} & C_{22} & C_{23} & 0 & 0 & 0 \\ C_{13} & C_{23} & C_{33} & 0 & 0 & 0 \\ 0 & 0 & 0 & C_{44} & 0 & 0 \\ 0 & 0 & 0 & 0 & C_{55} & 0 \\ 0 & 0 & 0 & 0 & 0 & C_{66} \end{bmatrix} \begin{Bmatrix} \varepsilon_{tt} - \alpha_1 \Delta T \\ \varepsilon_{nn} \\ \varepsilon_{bb} \\ \gamma_{nb} \\ \gamma_{tb} \\ \gamma_{tn} \end{Bmatrix} \quad (5)$$

where the C_{ij} can be found in Ref. [42].

The constitutive equation shown in above Eq. (5) for the beam can be further simplified based on the stress assumptions for a 3D beam. All stresses at the beam in the local coordinate system tnb are assumed to be negligible except $\sigma_t(\sigma_{tt})$, $\tau_n(\tau_{tn})$ and $\tau_b(\tau_{tb})$. However, all strains are not assumed to be zero. The stress-strain relation for the stiffener can be expressed as:

$$\begin{Bmatrix} \sigma_t \\ \tau_n \\ \tau_b \end{Bmatrix} = \begin{bmatrix} \bar{C}_{11} & 0 & 0 \\ 0 & \bar{C}_{66} & 0 \\ 0 & 0 & \bar{C}_{55} \end{bmatrix} \left(\begin{Bmatrix} \varepsilon_t \\ \gamma_n \\ \gamma_b \end{Bmatrix} - \begin{Bmatrix} \alpha_1 \Delta T \\ 0 \\ 0 \end{Bmatrix} \right) \quad (6)$$

where

$$\begin{aligned} \bar{C}_{55} &= C_{55}, \quad \bar{C}_{66} = C_{66} \\ \bar{C}_{11} &= \frac{C_{13}^2 C_{22} - 2C_{12}C_{13}C_{23} + C_{11}C_{23}^2 + C_{12}^2 C_{33} - C_{11}C_{22}C_{33}}{C_{23}^2 - C_{22}C_{33}} \end{aligned}$$

The matrix format for Eq. (6) is:

$$\boldsymbol{\sigma}_s = \bar{\boldsymbol{C}}(\boldsymbol{\varepsilon}_s - \boldsymbol{\varepsilon}_{s,T}) \quad (7)$$

where $\boldsymbol{\varepsilon}_{s,T}$ and $\boldsymbol{\varepsilon}_s$ are, respectively, thermal strain vector and elastic strain vector for the stiffener.

The strain given in Eq. (7) can be written as:

$$\boldsymbol{\varepsilon}_s = \boldsymbol{B}_s \boldsymbol{d}_s = \boldsymbol{B}_s \boldsymbol{T}_s \boldsymbol{N}_{sp} \boldsymbol{d}_p \quad (8)$$

where \boldsymbol{B}_s is the strain-displacement relation matrix and \boldsymbol{d}_s is the stiffener displacement described in the local coordinate system. The transformation matrix \boldsymbol{N}_{sp} is used to approximate the stiffener displacement in terms of the plate displacement based on the finite element shape functions for the isoparametric elements. The matrix of \boldsymbol{N}_{sp} can be computed using the geometry field for both the plate and stiffeners. This method was studied in detail in our previous work [24].

For completeness, a brief summary of the computation for the matrix \boldsymbol{N}_{sp} is presented. Figure 3 shows the j -th beam element, which is used to model the stiffener, passing through the i -th plate element. Both the displacement and geometry expressions for the node of the j -th beam element can be approximated in terms of those for the eight nodes of the i -th plate element based on the isoparametric elements used in the finite element method. Hence, the nodal displacement and geometry for each node ($m = 1, 2, 3$) of the j -th beam element can be expressed as:

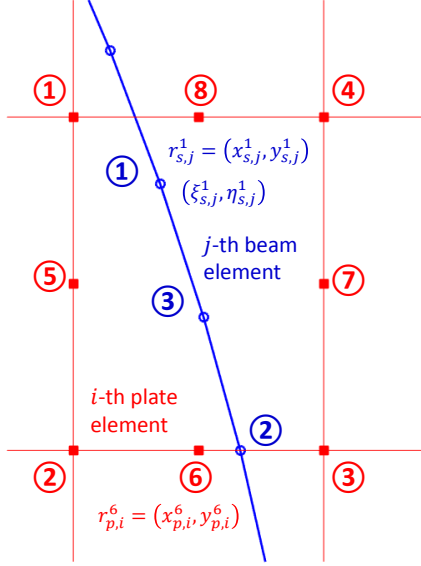


Figure 3: Approximation of stiffener beam element nodal displacement in term of those for the plate element

$$d_{sg,j}^m = \sum_{k=1}^8 N_{p,i}^k(\xi_{s,j}^m, \eta_{s,j}^m) d_{p,i}^k \quad (9a)$$

$$r_{s,j}^m = \sum_{k=1}^8 N_{p,i}^k(\xi_{s,j}^m, \eta_{s,j}^m) r_{p,i}^k \quad (9b)$$

where N_p is the shape function for an 8-noded shell element, and $(\xi_{s,j}^m, \eta_{s,j}^m)$ are natural coordinates for the m -th node of the j -th beam element within the i -th plate element as shown in Fig. 3 whose values can be computed using Eq. (9a). The computational time for solving these natural coordinates $(\xi_{s,j}^m, \eta_{s,j}^m)$ can be saved using parallel processing. The symbol i for the plate element is not shown in Eq. (9).

Based on this method, one can approximate all stiffener beam element nodal displacements and geometry fields using those for the plate. The geometry and displacement fields of the stiffener for the full model can be written in matrix forms as:

$$\mathbf{d}_{sg} = \mathbf{N}_{sp} \mathbf{d}_p, \quad \mathbf{r}_s = \mathbf{N}_{sp} \mathbf{r}_p \quad (10)$$

Note that \mathbf{d}_{sg} means the stiffener displacement described in the global coordinate system, which can be transformed to that described in the stiffener local coordinate system using a transformation matrix of \mathbf{T}_s . Also, since all stiffeners are modeled using composite beam elements, and all the beam element nodal displacements are approximated using that for the plate. The displacement compatibility conditions at the

stiffener/stiffener interfaces are satisfied automatically. Additionally, Eq. (10) can be used to derive the stiffener axial strain and stress [25], which can be used for stiffener sizing study considering yielding and crippling constraints. Considering the scope of the present paper is to study the effect of the VAT laminates and stiffener shape on the panel's buckling responses, the stiffener's yielding and crippling constraints are not considered in the present work but will be considered in future work.

Mesh examples of a stiffened plate with four arbitrarily shaped stiffeners are shown in Fig. 4 to demonstrate the benefit of the present method. When there is a change in a stiffener's shape, the conventional finite element method needs to re-mesh the structure for the analysis in both the plate and the stiffeners, as shown in Figs. 4a and 4c. The present method only needs to re-mesh the stiffener when the shape is changed, as seen in Figs. 4b and 4d. To avoid a meshing failure, a small mesh size is normally used during stiffener shape optimization using previously developed panel optimization code, EBF3PanelOpt [28]. However, there is no need to use fine mesh for the present model as the plate and the stiffeners are modeled separately.

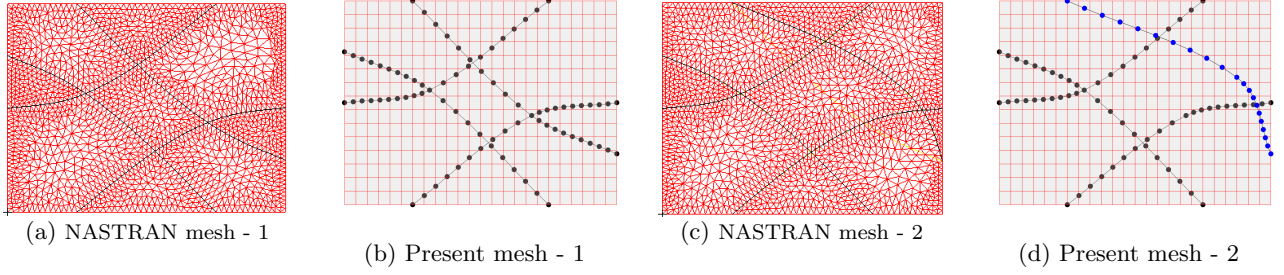


Figure 4: Mesh examples of a stiffened plate with arbitrarily shaped stiffeners

Based on the stress-strain relation for the stiffener given in Eq. (7), the total potential energy for the stiffeners is

$$\begin{aligned} \Pi_s &= \frac{1}{2} \iiint_V (\varepsilon_s - \varepsilon_{s,T})^T \bar{C}^T (\varepsilon_s - \varepsilon_{s,T}) dV \\ &= \frac{1}{2} \iiint_V (\varepsilon_s^T \bar{C}^T \varepsilon_s - 2\varepsilon_s^T \bar{C}^T \varepsilon_{s,T} + \varepsilon_{s,T}^T \bar{C}^T \varepsilon_{s,T}) dV \\ &= \frac{1}{2} \iiint_V \left(d_p^T N_{sp}^T T_s^T B_s^T \bar{C}^T B_s T_s N_{sp} d_p - 2d_p^T N_{sp}^T T_s^T B_s^T \bar{C}^T \varepsilon_{s,T} + \varepsilon_{s,T}^T \bar{C}^T \varepsilon_{s,T} \right) dV \end{aligned} \quad (11)$$

B. Thermo-elastic Analysis

The total strain energy for the stiffened plate subjected to the thermal load is obtained by summing the plate strain energy given in Eq. (4) and stiffeners' strain energy shown in Eq. (11) as:

$$\begin{aligned}
\Pi &= \Pi_p + \Pi_s \\
&= \frac{1}{2} \iiint_V \left(\mathbf{d}_p^T \mathbf{B}^T \bar{\mathbf{Q}}^T \mathbf{B} \mathbf{d}_p - 2 \mathbf{d}_p^T \mathbf{B}^T \bar{\mathbf{Q}}^T \boldsymbol{\varepsilon}_T + \boldsymbol{\varepsilon}_T^T \bar{\mathbf{Q}}^T \boldsymbol{\varepsilon}_T \right) dV + \\
&\quad \frac{1}{2} \iiint_V \left(\mathbf{d}_p^T \mathbf{N}_{sp}^T \mathbf{T}_s^T \mathbf{B}_s^T \bar{\mathbf{C}}^T \mathbf{B}_s \mathbf{T}_s \mathbf{N}_{sp} \mathbf{d}_p - 2 \mathbf{d}_p^T \mathbf{N}_{sp}^T \mathbf{T}_s^T \mathbf{B}_s^T \bar{\mathbf{C}}^T \boldsymbol{\varepsilon}_{s,T} + \boldsymbol{\varepsilon}_{s,T}^T \bar{\mathbf{C}}^T \boldsymbol{\varepsilon}_{s,T} \right) dV
\end{aligned} \tag{12}$$

The thermo-elastic governing equation for computing the stress distribution for the plate and the stiffeners can be obtained from the minimum total potential energy principle, $\delta\Pi = 0$

$$\begin{aligned}
\delta\Pi &= \delta \left(\frac{1}{2} \iiint_V \left(\mathbf{d}_p^T \mathbf{B}^T \bar{\mathbf{Q}}^T \mathbf{B} \mathbf{d}_p \right) dV \right) - \delta \left(\iiint_V \mathbf{d}_p^T \mathbf{B}^T \bar{\mathbf{Q}}^T \boldsymbol{\varepsilon}_T dV \right) + \delta \left(\iiint_V \mathbf{d}_p^T \mathbf{B}^T \bar{\mathbf{Q}}^T \boldsymbol{\varepsilon}_T dV \right)^0 \\
&\quad - \delta \left(\frac{1}{2} \iiint_V \mathbf{d}_p^T \mathbf{N}_{sp}^T \mathbf{T}_s^T \mathbf{B}_s^T \bar{\mathbf{C}}^T \mathbf{B}_s \mathbf{T}_s \mathbf{N}_{sp} \mathbf{d}_p dV \right) - \delta \left(\iiint_V \mathbf{d}_p^T \mathbf{N}_{sp}^T \mathbf{T}_s^T \mathbf{B}_s^T \bar{\mathbf{C}}^T \boldsymbol{\varepsilon}_{s,T} dV \right) + \delta \left(\frac{1}{2} \iiint_V \mathbf{d}_p^T \mathbf{N}_{sp}^T \mathbf{T}_s^T \mathbf{B}_s^T \bar{\mathbf{C}}^T \boldsymbol{\varepsilon}_{s,T} dV \right)^0
\end{aligned} \tag{13}$$

There are two terms to be zero in Eq. (13) because they are independent of the panel elastic displacement.

Based on Eq. (13), the thermo-elastic governing equation is obtained as:

$$[\mathbf{K}_p + \mathbf{K}_s] \mathbf{d}_p = \mathbf{F}_T \tag{14}$$

where

$$\begin{aligned}
\mathbf{K}_p &= \iiint_V \mathbf{B}^T \bar{\mathbf{Q}}^T \mathbf{B} dV = \iint_{\Omega} \mathbf{B}^T \mathbf{D}_p^T \mathbf{B} dx dy \\
\mathbf{K}_s &= \iiint_V \mathbf{N}_{sp}^T \mathbf{T}_s^T \mathbf{B}_s^T \bar{\mathbf{C}}^T \mathbf{B}_s \mathbf{T}_s \mathbf{N}_{sp} dV = \int_{\Gamma} \mathbf{N}_{sp}^T \mathbf{T}_s^T \mathbf{B}_s^T \mathbf{D}_s^T \mathbf{B}_s \mathbf{T}_s \mathbf{N}_{sp} ds \\
\mathbf{F}_T &= \iiint_V \left(\mathbf{B}^T \bar{\mathbf{Q}}^T \boldsymbol{\varepsilon}_T + \mathbf{N}_{sp}^T \mathbf{T}_s^T \mathbf{B}_s^T \bar{\mathbf{C}}^T \boldsymbol{\varepsilon}_{s,T} \right) dV = \iint_{\Omega} \mathbf{B}^T \mathbf{D}_p^T \boldsymbol{\varepsilon}_{p,T} dx dy + \int_{\Gamma} \mathbf{N}_{sp}^T \mathbf{T}_s^T \mathbf{B}_s^T \mathbf{D}_s^T \boldsymbol{\varepsilon}_{s,T} ds
\end{aligned}$$

Note that we use s in \mathbf{K}_s and \mathbf{F}_T to represent stiffener longitudinal direction parameter. The matrices given in these stiffness expressions are not shown here for brevity, which can be found in our previous work [24].

The stiffness matrices can be evaluated using Gaussian quadrature when using the finite element method. The fiber path angle for each layer of each element is evaluated at the element center. The element stiffness matrices, \mathbf{K}_p^e and \mathbf{K}_s^e , respectively, are:

$$\begin{aligned}
\mathbf{K}_p^e &= \int_{-1}^{+1} \int_{-1}^{+1} \mathbf{B}_p^T \mathbf{D}_p(\boldsymbol{\theta})^T \mathbf{B}_p \det \mathbf{J}_p d\xi d\eta \\
\mathbf{K}_s^e &= \int_{-1}^{+1} \mathbf{N}_{sp}^T \mathbf{T}_s^T \mathbf{B}_s^T \mathbf{D}_s^T \mathbf{B}_s \mathbf{T}_s \mathbf{N}_{sp} \det \mathbf{J}_s d\xi
\end{aligned} \tag{15}$$

C. Thermal Buckling Analysis

For thermal buckling studied in this paper, the geometric stiffness for both plate and stiffeners are computed in terms of the computed stress distributions for the plate and stiffeners, respectively, using Eqs. (3) and (7). Note that the values of strain-displacement relations for the plate \mathbf{B}_p and the stiffeners \mathbf{B}_s are different when computed at different Gaussian integration points. In this work, the in-plane strains for the plate, $\boldsymbol{\varepsilon}_p$, and stiffeners, $\boldsymbol{\varepsilon}_t$, are obtained by averaging the strain components that are computed at Gauss integration points [43].

Once we obtain the stress resultants distribution for the plate and the stiffeners using Eqs. (3) and (7), respectively. We can compute the geometric stiffness matrices for the plate and stiffeners. For brevity, the formulations for the geometric stiffness for both the plate and the stiffeners are not shown. However, they can be found in our previous work [24]. An eigenvalue analysis is conducted for the following equation for the buckling load factor, λ_b :

$$[(\mathbf{K}_p + \mathbf{K}_s) + \lambda_b (\mathbf{K}_{Gp} + \mathbf{K}_{Gs})] \{\mathbf{u}_p\} = \mathbf{0} \quad (16)$$

where \mathbf{K}_{Gp} and \mathbf{K}_{Gs} are the differential stiffness matrices for the panel and the stiffeners due to the in-plane stresses, respectively; λ_b is buckling load factor and the corresponding buckling mode shape is $\{\mathbf{u}_p\}$.

The element differential stiffness matrices, \mathbf{K}_{Gp}^e and \mathbf{K}_{Gs}^e , respectively, are

$$\begin{aligned} \mathbf{K}_{Gp}^e &= \int_{-1}^{+1} \int_{-1}^{+1} \left(\mathbf{B}_p^{NL} \right)^T \boldsymbol{\sigma}_p(\boldsymbol{\theta})^T \mathbf{B}_p^{NL} \det \mathbf{J}_p d\xi d\eta \\ \mathbf{K}_{Gs}^e &= \int_{-1}^{+1} \mathbf{N}_{sp}^T \mathbf{T}_s^T \left(\mathbf{B}_s^{NL} \right)^T \boldsymbol{\sigma}_s \mathbf{B}_s^{NL} \mathbf{T}_s \mathbf{N}_{sp} \det \mathbf{J}_s d\xi \end{aligned} \quad (17)$$

where \mathbf{J}_p and \mathbf{J}_s are the Jacobians for the panel and the stiffener, respectively, both of which are given in Ref. [24]. The integration required for the stiffness matrix calculations for the composite panel and the composite stiffeners are performed using Gaussian quadrature.

III. Geometry Parameterization for Curvilinear Stiffener

Both the straight and curved stiffeners are considered in this work. To generate such curves, Hobby spline [38] is used to parameterize the arbitrarily shaped stiffeners in any physical space. This is because the Non-Uniform Rational Basis Spline (NURBS) curves used in previous works [24, 27] do not pass through all control points, which make it inconvenient to use locations of control points to determine the shape of

stiffeners. An additional step is often needed to check whether the parameterized stiffener is located within the plate or not when using NURBS for stiffener shape parameterization. Hobby spline allows the curve to pass through all control points as shown in Fig. 5, which could satisfy the constraints on the locations of parameterized curves in the surface without the need for the additional location check. Additionally, Hobby spline allows local change in the curve without the effect on the global shape while the polynomials change the curve global shape.

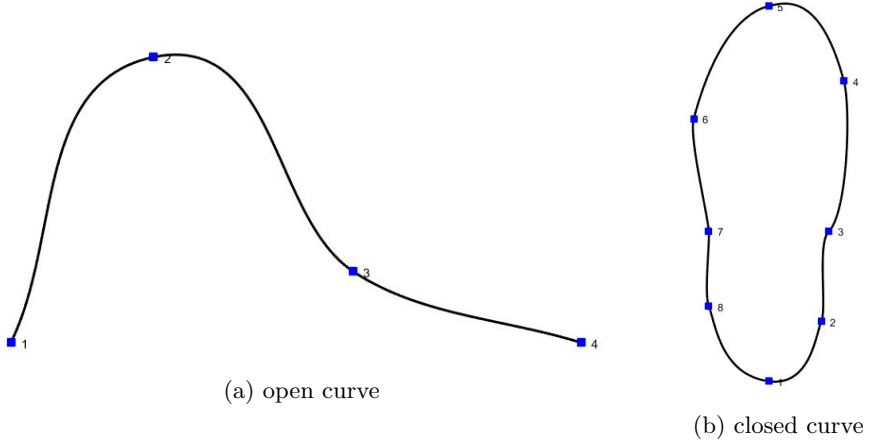


Figure 5: Two examples of Hobby spline [38]

The parameterization of an arbitrarily shaped curve lying inside a surface has been studied in previous works by the present authors [23, 24, 27, 44]. Both three- and four-noded NURBS curves are used. Note that more the number of control points, more the number of design variables. In this paper, we use three control points to define the shape of an arbitrarily shaped curve. The start and end control points are determined from the placement parameters and the middle point is parameterized using a shape parameter.

A. Placement parameter

The parameterization on the placement has been presented in detail in our previous work; however, for completeness, we briefly present the method in this section. To reduce the number of the shape design variables, the start and end points, A and B, are parameterized by a perimeter parameter, ε , starting from 0 to 1 as shown in Fig. 6. The perimeter parameter for each point, A or B, is then transformed to a natural space which is used in the finite element method. This transformation uses the advantage of the shape functions ($N_{1,2,3,4}$) for a four-noded quadrilateral shell element, so that it works for any shaped quadrilateral plate. The natural coordinates for the start and end points can be obtained from Table 1. One of the four edges could be collapsed, so that the method works for a triangular plate.

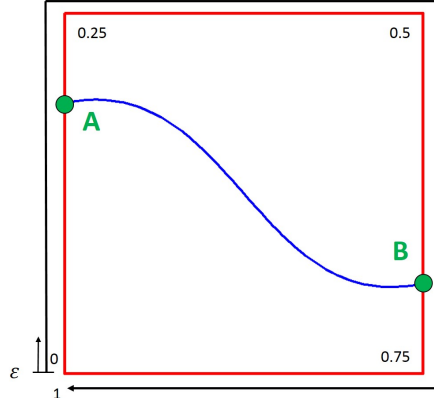


Figure 6: Parameterization of start and end point locations, points A and B

Table 1: The relationship between the perimeter parameter, ε , and the natural coordinates, ξ and η

ε	ξ	η
$[0, 0.25]$	-1	$-1+8\varepsilon$
$[0.25, 0.50]$	$-1+8(\varepsilon - 0.25)$	1
$[0.50, 0.75]$	1	$-8(\varepsilon - 0.5) + 1$
$[0.75, 1.00]$	$-1-8(\varepsilon - 1)$	-1

The physical coordinate for the start and end points, A and B, in the physical space are:

$$\begin{aligned} x_A &= N_1(\xi_A, \eta_A)x_1 + N_2(\xi_A, \eta_A)x_2 + N_3(\xi_A, \eta_A)x_3 + N_4(\xi_A, \eta_A)x_4 \\ y_A &= N_1(\xi_A, \eta_A)y_1 + N_2(\xi_A, \eta_A)y_2 + N_3(\xi_A, \eta_A)y_3 + N_4(\xi_A, \eta_A)y_4 \\ x_B &= N_1(\xi_B, \eta_B)x_1 + N_2(\xi_B, \eta_B)x_2 + N_3(\xi_B, \eta_B)x_3 + N_4(\xi_B, \eta_B)x_4 \\ y_B &= N_1(\xi_B, \eta_B)y_1 + N_2(\xi_B, \eta_B)y_2 + N_3(\xi_B, \eta_B)y_3 + N_4(\xi_B, \eta_B)y_4 \end{aligned} \quad (18)$$

where $x_{1,2,3,4}$ and $y_{1,2,3,4}$ are physical coordinates of the four vertices of a quadrilateral plate. One can refer to [44] for more details.

B. Shape parameter

The shape of an arbitrarily shaped stiffener was parameterized using a distance where the middle control point moves perpendicular to the line between the start and the end points [24, 44]. This moving distance depends on the start and end points locations for defining the middle control point location. It is hard to set the upper and lower bounds for such shape parameters in an optimization study. In this work, we use the natural coordinates, (ξ, η) , as shown in Eq. (18) to quantify the location of the middle control point. As long as the constraint of $-1 \leq (\xi, \eta) \leq 1$ is satisfied, the middle control point is located in the panel. One can use Eq. (18) to obtain its physical coordinates, (x_C, y_C) , in surface using the natural coordinates (ξ_C, η_C) . The physical coordinates for the three control points are used to generate the stiffener curve by using Hobby spline.

In summary, for one curve parameterized using the present approach, there are four shape design variables including two perimeter parameters for the start and end points and two natural coordinates for the middle

control point. There is still a chance that some parts of the curve generated using Hobby spline are located outside the physical space. Nevertheless, as compared to that using NURBS, the present parameterization approach allows one to have same upper and lower bounds, $[-1, 1]$, for all shape parameters. The NURBS curve is located in the polygons generated by the control points, it is possible to have a NURBS curve located in the physical space while the middle control point is outside the physical space. This leads to a difficulty in defining upper and lower bounds for all shape parameters, when using NURBS for parameterizing curvilinear stiffeners shape, in shape optimization. This difficulty can be overcome when using Hobby spline for parameterizing the curvilinear stiffeners. Additionally, the present method uses area equal method to determine the stiffener element node locations [24, 25]. For a stiffener point located in the plate, the lines between the stiffener point and the plate vertices divide the plate into four small triangles. The area equal method means that when the sum of the areas for the four triangles equals the area for the plate, the node is located in the plate otherwise outside the plate. When one stiffener element node is outside the surface, the area equality constraint is not satisfied. This method can be used to quantify the stiffener shape parameter violation in the shape optimization.

IV. Thermal Buckling of Composite Panel

The section verifies the present program in thermal buckling analysis of a composite panel with both straight and curvilinear fibers. Both uniform and nonuniform temperature gradients are studied in this section. Note that the temperature used in the present work represents the temperature change or temperature gradient, ΔT ; for convenience, the buckling temperature shown in the following sections represents the buckling temperature gradient.

A. Uniform Temperature for Composite Panel with Straight Fibers

A simply-supported rectangular composite panel with aspect ratio ($a/b = 1.25$) with dimensions of $(a \times b \times h) = (15 \times 12 \times 0.048)m$. For verification studies, the material properties are chosen to be the same as those in Ref [12, 13, 45]: $E_1 = 22.5\text{MPa}$, $E_2 = 1.17\text{MPa}$, $G_{12}=0.66\text{MPa}$, $\nu_{12}=0.22$ and thermal expansion coefficients $\alpha_1 = -0.04 \times 10^{-6}(1/\text{ }^{\circ}\text{C})$ and $\alpha_2 = 16.7 \times 10^{-6}(1/\text{ }^{\circ}\text{C})$. The layer thickness is 6 mm. Both symmetrically cross-ply and angle-ply laminated panels are studied, in both convergence and verification studies as shown in Table 2. It can be seen that for both cases, the results converge with the plate mesh size. Also, the converged results match well with the results available in literature. Since the shear deformation is considered in the present analysis, the obtained results are slightly lower than the results obtained without

including shear deformation.

Table 2: Convergence and verification studies on thermal buckling of a composite panel under a uniform temperature

Laminates \ Mesh	8×6	12×8	18×12	24×18	32×24	Shi <i>et al.</i> [45]	Shiau <i>et al.</i> [12]	Ounis <i>et al.</i> [13]
$[0/90/90/0]_s$	12.23	12.24	12.25	12.25	12.25	12.26	12.26	12.26
$[0/45/-45/90]_s$	13.62	13.64	13.65	13.65	13.65	13.71	13.75	13.74

B. Non-Uniform Temperature for Composite Panel with Straight Fibers

A simply-supported rectangular composite panel used by Meyers and Hyer [46] is employed here to verify the present program in thermal buckling analysis under nonuniform temperature change. The material properties are given in Ref. [46] as : $E_1 = 155.0\text{GPa}$, $E_2 = 8.07\text{GPa}$, $G_{12}=4.55\text{MPa}$, $\nu_{12}=0.22$ and thermal expansion coefficients $\alpha_1 = -0.07 \times 10^{-6}(1/\text{°C})$ and $\alpha_2 = 30.1 \times 10^{-6}(1/\text{°C})$. The layer thickness is $1.272 \times 10^{-4} \text{ m}$. The temperature change ΔT is given by,

$$\Delta T = \lambda_T \left(1 + \bar{T} \frac{z}{H} \right) \quad (19)$$

where λ_T is the factor for the temperature change at the midplane of the plate, H is the total panel thickness, z is the thickness coordinate, and \bar{T} controls the magnitude of the through-the-thickness gradient. When the value of \bar{T} is positive, it means the top side is warmer than the bottom side. In this verification study case, $\bar{T} = 0.05$.

Mesh convergence study on the thermal buckling load for the quasi-isotropic square composite panel subjected to a nonuniform temperature change was conducted as shown in Table 3. It is seen that the results change slightly with the mesh size. The converged result using a mesh size of 18×18 for the panel matches well with the reference result.

Table 3: Convergence and verification studies on buckling temperature of a square composite panel, $a = b = 0.15 \text{ m}$, quasi-isotropic laminate configuration $[\pm 45/0/90]_s$

Mesh size	8×8	12×12	18×18	24×24	36×36	Meyers and Hyer [11]
Buckling temperature, °C	38.54	38.53	38.52	38.51	38.51	38.6

Considering the possible skew angle of the material axes relative to the edge of the plate [11], a parametric study on the buckling temperature in terms of various skew angles is conducted. The skew angle is defined

by rotating all fiber plies about the z -axis by one angle, α , in a counter-clockwise direction. If the skew angle is $\alpha = 30$ degrees, for example, then the $[\pm 45/0_2]_s$ laminates become the fiber ply orientations of $[+75/-15/30_2]_s$.

The mesh size for the plate is 18×18 . Two different plate aspect ratios for the plate, $a/b = 1$ and $a/b = 2$, are studied with a fixed width, $b = 0.15\text{m}$. Figure 7 shows the predicted results match very well with the results available in literature [11] where $\Delta T^* = 38.52^\circ\text{C}$ is buckling temperature for the square quasi-isotropic composite panel with zero skew angle. It is observed from Fig. 7 that the square panel has a larger buckling temperature than that of the rectangular panel. The skew angle decreases the buckling temperature for the square panel ($a/b = 1$) by more than 20% while the positive skew angle leads to a $\sim 10\%$ increase in the buckling temperature for the rectangular panel ($a/b = 2$) at the studied skew angle range up to 30 degrees.

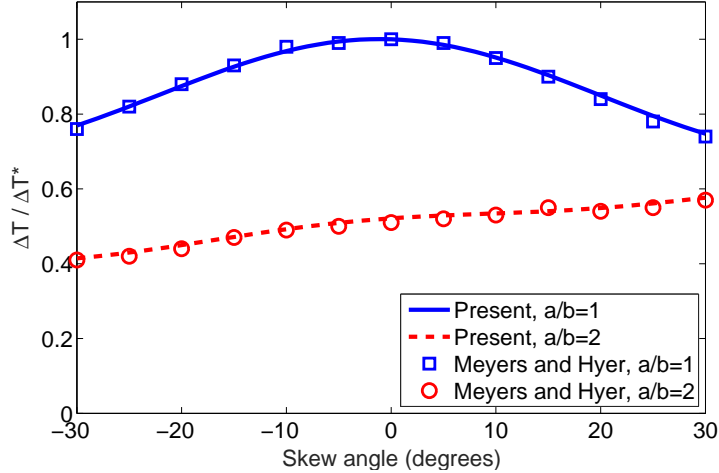


Figure 7: Buckling temperature with skew angle, α

C. Uniform Temperature for VAT Laminated Panel

In this case, a uniform temperature change is considered for a simply-supported VAT laminated panel studied by Duran *et al.* [16] to verify the present program on thermal buckling analysis on VAT laminated plates. A square composite panel with side length of $a = 0.15\text{m}$ and the thickness of $h = 1.016\text{mm}$ is considered. A four-layer symmetric laminate configuration $(\pm\theta_0|\theta_1)_s$ is used. Different materials for the VAT laminates are studied whose properties can be found in Table 4.

The present results in thermal buckling temperature for all material cases agree well with those obtained by Duran *et al.* [16] as shown in Table 5 except the results for Cases (d) and (e). Both NASTRAN and

ABAQUS are also used to compute the thermal buckling temperatures as shown in Table 5. Since NASTRAN and ABAQUS have no capabilities of modeling the curvilinear fibers for the laminated composites directly, we used a fine mesh for developing the finite element model for the plate where each element is assumed to have laminates with straight fibers. The straight fiber path angle for each layer of each element is evaluated at the element's center using Eq. 1. A relatively fine 4-noded quadrilateral mesh is consider for the plate, 100×100 , for both NASTRAN and ABAQUS to ensure the converged results obtained from the subsequent comparison.

The present buckling temperatures agree very well with NASTRAN and ABAQUS results for all cases. The buckling mode shapes for all cases computed using the present method compare well with those computed using ABAQUS and NASTRAN. For brevity, the mode shape comparisons are shown in the supplemental material. The discrepancy between the present results with those obtained by Duran *et al.* [16] is because Duran *et al.* only consider the thermal induced stress in computing the geometric stiffness for buckling analysis. The elastic strain for the plate ε_p in Eq. (3) and, ε_s for the stiffeners in Eq. (7) were not considered for computing the in-plane stress resultants when using that method. Our previous work [47] followed that method as presented by Duran *et al.* [16] and found that all computed buckling temperatures agree well with those by Duran *et al.* [16]. That method only works for the case when the induced elastic strain by the restrained thermal expansion, ε_p , is much less than the thermal strain, $\varepsilon_{p,\Delta T}$. However, the elastic strain induced stress resultants are too large to be ignored for the present VAT laminated plate. The present code for this example is available in GitHub (https://github.com/zhaowei0566/Thermal_VAT).

Table 4: Material properties

Case	Material	E_1 (GPa)	E_2 (GPa)	G_{12} (GPa)	μ_{12}	α_1 ($1/^\circ\text{C}$) 10^{-6}	α_2 ($1/^\circ\text{C}$) 10^{-6}
(a)	Graphite/Epoxy	155	8.07	4.55	0.22	-0.07	30.1
(b)	E-Glass/Epoxy	41.	10.04	4.3	0.28	7.0	26.
(c)	S-Glass/Epoxy	45.	11.0	4.5	0.29	7.1	30.
(d)	Kevlar/Epoxy	80.	5.5	2.2	0.34	-2.0	60
(e)	Carbon/Epoxy	147.	10.3	7.0	0.27	-0.9	27
(f)	Carbon/Peek	138	8.7	5.0	0.28	-0.2	24
(g)	Carbon/Polyimide	216	5.0	4.5	0.25	0.0	25
(h)	Boron/Epoxy	201.	21.7	5.4	0.17	6.1	30.

Table 5: Comparisons of buckling temperature for square VAT laminated panel with different materials, $(\pm\langle\theta_0|\theta_1\rangle)_s$

Case	Material	$\langle\theta_0 \theta_1\rangle$ (degrees)	ΔT_{crit} (°C) (Ref. [16])	Present (°C)	Diff.	NASTRAN °C (Diff.)	ABAQUS °C (Diff.)
(a)	Graphite/Epoxy	$\langle 60.70 32.19 \rangle$	34.26	31.99	-6.63%	32.66 (-2.05%)	31.91 (0.25%)
(b)	E-Glass/Epoxy	$\langle 6.71 58.04 \rangle$	5.58	5.48	-1.79%	5.54 (-1.08%)	5.47 (0.18%)
(c)	S-Glass/Epoxy	$\langle 16.12 54.74 \rangle$	5.04	4.96	-1.51%	5.03 (-1.31%)	4.96 (0.08%)
(d)	Kevlar/Epoxy	$\langle 66.05 11.73 \rangle$	22.18	16.09	-27.46%	16.27 (-1.11%)	16.06 (0.19%)
(e)	Carbon/Epoxy	$\langle 69.00 - 5.705 \rangle$	57.79	33.80	-41.51%	35.32 (-4.30%)	33.76 (0.12%)
(f)	Carbon/PEEK	$\langle 63.07 29.50 \rangle$	38.08	34.93	-8.27%	35.54 (-1.72%)	34.85 (0.23%)
(g)	Carbon/Polyimide	$\langle 56.30 36.68 \rangle$	78.28	74.89	-4.33%	76.89 (-2.60%)	74.61 (0.38%)
(h)	Boron/Epoxy	$\langle -6.57 63.28 \rangle$	7.50	7.35	-2.00%	7.53 (-2.39%)	7.32 (0.41%)

V. Thermal Buckling of Curvilinearly Stiffened VAT Laminates

This section first verifies the present program in computing thermal buckling load for a curvilinearly stiffened VAT laminated plate. After that, a parametric study is conducted for a stiffened VAT laminated plate with straight stiffeners. A linearly varying fiber path is considered for the VAT laminated plate. The effect of stiffener shape on the thermal buckling load is also studied through a parametric study. An optimization study is conducted in this section for maximizing the buckling temperature in terms of stiffener shape and size variables and VAT laminate fiber path orientations. The weight constraint is considered in this optimization study.

A. Verification Study

The square panel studied in Section IV-C is used for verifying the thermal buckling of a curvilinearly stiffened laminated plate subjected to a uniform temperature, $\Delta T = 1$ °C. The physical coordinates for curves ① and ②, generated using the geometric parameterization method presented in Section III, are given in Appendix A. Note that NASTRAN uses Bspline to fit a curve from a number of discrete points up to 10 rather than using the Hobby spline. To ensure that the stiffener beam nodal coordinates used in the present model are consistent with that in NASTRAN, the physical points for the two stiffeners are created in NASTRAN and they are used to generate the stiffener curves using NASTRAN built-in Bspline tool. The finite element nodes for the stiffener beam elements used in NASTRAN are also used in the present model for stiffeners in the subsequent buckling verification study.

The geometric dimensions for both the plate and the stiffeners are described in Fig. 8. An eight-layer symmetric VAT laminate configurations of $(\pm 69^\circ| - 5.705^\circ)_{2,s}$ is considered. The layer thickness is 1.27E-4

m. The stiffeners are modeled as orthotropic beams which are equivalent to laminated beam with zero fiber path degree. Carbon/Epoxy is considered for both the plate and stiffeners, whose material properties are given in Table 4.

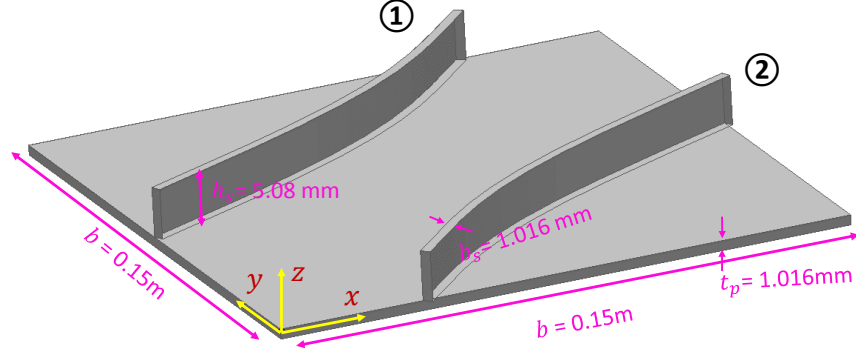


Figure 8: Stiffened VAT laminated plate with two curvilinear stiffeners

Since there is no available result in literature regarding thermal buckling of curvilinearly stiffened VAT laminated plates, NASTRAN results are used to verify the present program regarding thermal buckling analysis. Both concentric and eccentric stiffeners are considered. Note that this work is not to compare the computing efficiency of the two methods but to verify the present program using NASTRAN results. To get a converged result for the subsequent comparison, a relatively fine mesh is considered for the NASTRAN model that employs 5322 triangular elements (CTRIA3) for the plate and 100 beam elements (CBEAM) for each stiffener as shown in Fig. 9a.

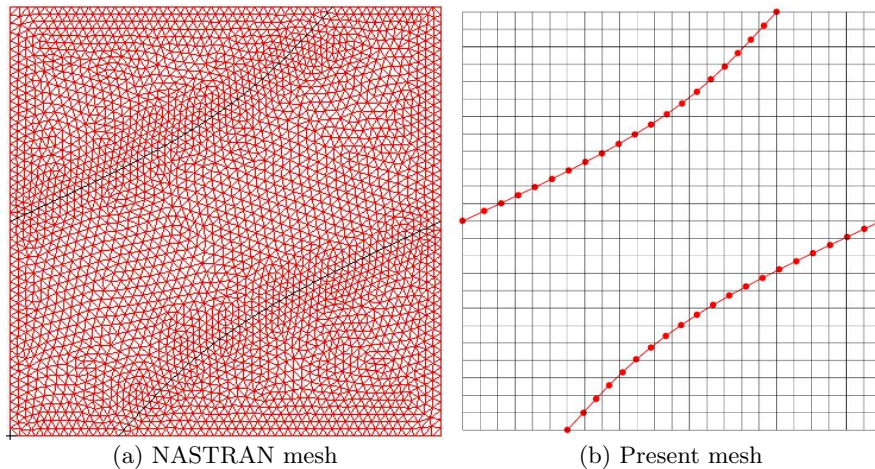


Figure 9: Finite element models used in NASTRAN and present program

Note that the glue contact cannot be used for the stiffened plate when there exist offsets in the beam models and the plate elements when using NASTRAN because the eccentric stiffeners are modeled as beam elements. Another reason of using a relatively fine mesh for the curvilinearly stiffened plate when using NASTRAN is that the fine mesh is often used to avoid the meshing failure. The convergence and verification studies regarding the thermal buckling for the unstiffened plate are conducted first. However, for brevity, they are not shown here as Section IV has already studied the thermal buckling for the unstiffened plate in detail. A converged mesh for the plate of 24×24 is considered in the present analysis as shown in Fig. 9b.

Table 6: Mesh convergence and verification studies of buckling temperature (ΔT_{cr}) of stiffened laminated plate with each stiffener beam elements number, plate mesh size: 24×24 (unit: $^{\circ}\text{C}$)

Mode	Concentric stiffeners					Eccentric stiffeners				
	No.	10	20	40	NASTRAN	Diff.	10	20	40	NASTRAN
1	77.67	77.75	77.78	78.00	-0.31%	100.48	100.93	101.03	100.92	0.01%
2	117.20	117.41	117.44	118.07	-0.56%	122.19	122.61	122.61	123.27	-0.53%
3	138.37	138.70	138.78	140.06	-0.97%	149.86	150.00	150.08	152.25	-1.48%
4	142.85	143.05	143.09	144.65	-1.11%	151.53	151.69	151.75	153.83	-1.39%
5	149.77	149.89	149.92	151.97	-1.37%	159.46	159.99	160.01	162.38	-1.47%
6	158.81	159.14	159.22	161.87	-1.68%	165.03	165.54	165.55	168.37	-1.68%
7	171.99	172.31	172.39	175.25	-1.68%	191.28	191.52	191.65	196.25	-2.41%
8	183.83	184.18	184.28	188.79	-2.44%	191.70	191.92	192.01	196.75	-2.45%
9	192.30	192.43	192.47	197.64	-2.63%	204.42	205.22	205.26	210.70	-2.60%
10	210.64	211.28	211.38	216.93	-2.60%	214.51	215.26	215.29	222.37	-3.20%

Table 6 shows the convergence and verification studies on the buckling temperature for a curvilinearly stiffened plate with the stiffener mesh size. For buckling analysis, we are often interested in only the first buckling mode. In the verification studies, for both stiffener cases, the eigenvalues for the first 10 buckling modes are examined. It is observed that there is a less than 1% change in all the eigenvalues when doubling the stiffener beam elements number from 20 to 40 for each stiffener. The buckling eigenvalues for both cases are found to converge with the stiffener beam elements number. The thermal buckling temperatures for both cases are computed using 20 beam elements for each stiffener and both results are found to be in a good agreement with the NASTRAN results. The mode shapes for the first two buckling modes obtained from the present analysis are compared with the NASTRAN results and a good agreement is observed between them as shown in Fig. 10. Based on this verification work, along with the verification works in Section IV regarding the thermal buckling of unstiffened VAT laminates, it can be concluded that the present program can accurately predict the thermal buckling for the curvilinearly stiffened VAT laminated plate.

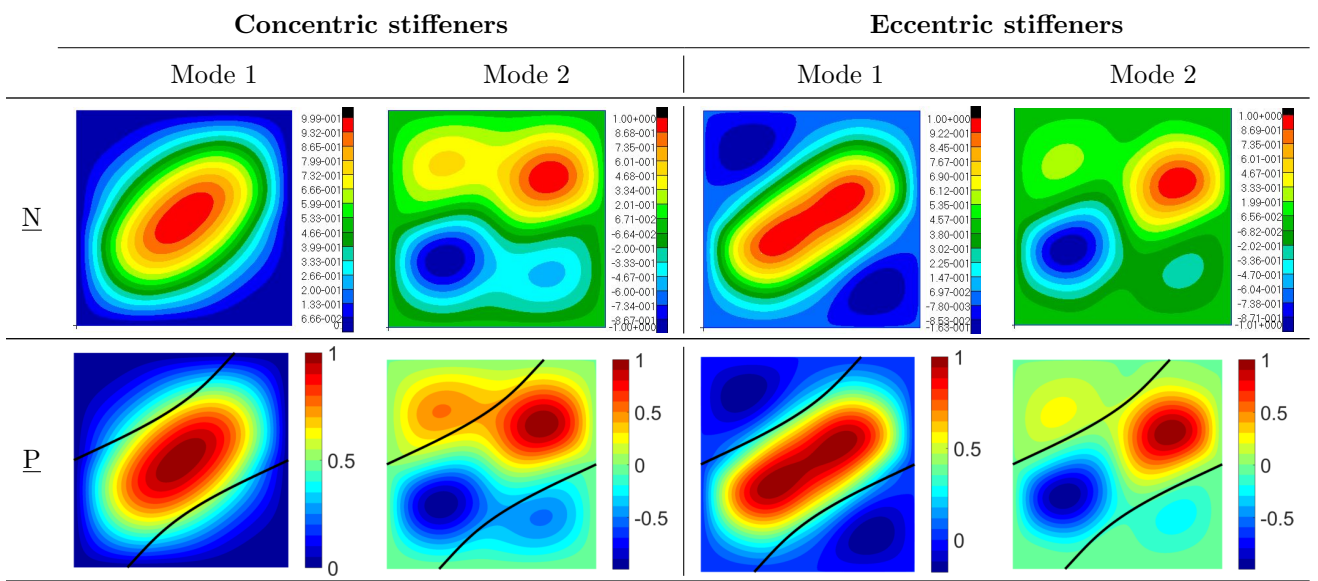


Figure 10: First two buckling mode shapes of a curvilinearly stiffened plate. N: NASTRAN results; P: present results

B. Straight Stiffeners

The model studied in Section IV-C along with the composite material, Carbon/Epoxy (see Table 4 for material properties), used by Duran *et al.* [16], are considered in this section. For launch vehicle panels subjected to aerodynamic load during cruising, its spanwise direction axial force is much larger than others. Hence, two straight equidistant stiffeners [48] are normally considered along the panel width direction, which are placed at $y = b/3$ and $y = 2b/3$, as shown in Fig. 11. The stiffened plate is used to study the buckling for stiffened VAT laminates under a uniform temperature change, $\Delta T = 1^\circ\text{C}$. The square composite panel has an 8-layer laminate configuration of $(\pm[\langle\Theta_0|\Theta_1\rangle_2])_s$. The layer thickness is $1.27 \times 10^{-4}\text{m}$. A linear fiber ply orientation for the VAT laminates is given as shown in Eq. (1). The material properties for both the laminated plate and the orthotropic stiffeners are same. The stiffener depth ratio is fixed as $h_s/b_s = 5$ and the stiffener width, b_s , equals the panel thickness. Simply-supported boundary conditions are considered for the studied model where the three displacements, u , v and w , are zero at the panel's four edges.

Buckling temperature with the fiber ply orientations for the unstiffened plate, the stiffened plates with two concentric stiffeners and two eccentric stiffeners are shown in Fig. 12. The diagonal line in white means the buckling temperature for the plate with the straight fiber path laminates. It is clearly observed that VAT laminates can improve the buckling temperature for all cases. The maximum buckling temperature and its corresponding optimal laminates are shown in Table 7.

As expected, a significant increase in the total buckling temperature using stiffeners is observed. The

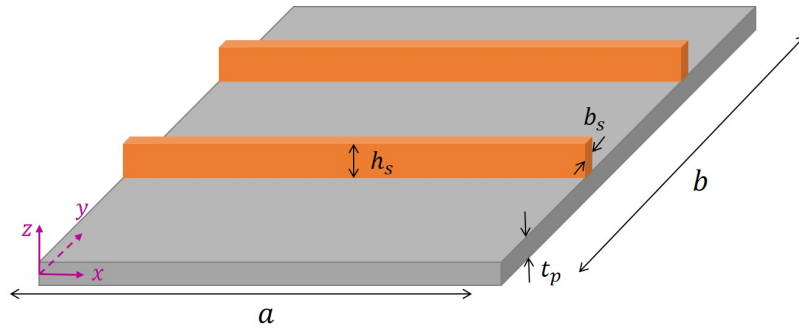


Figure 11: Stiffened plate with two straight stiffeners

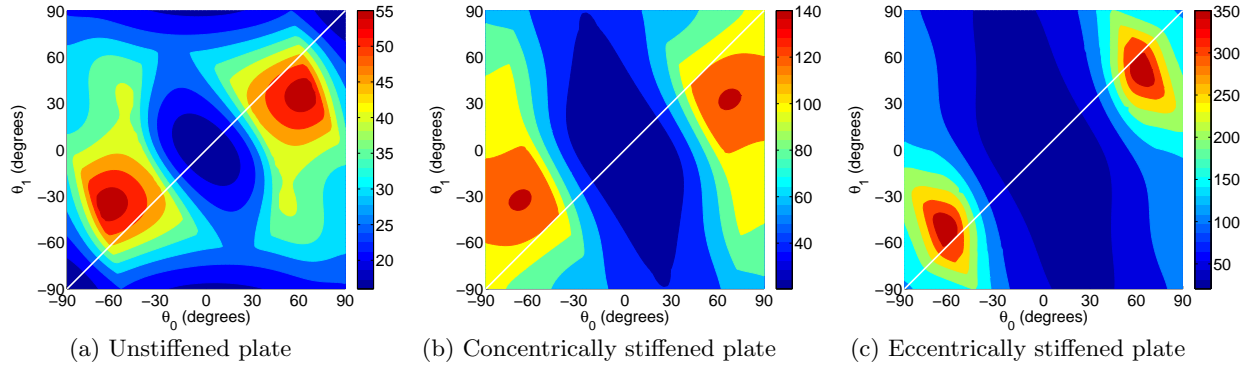


Figure 12: Thermal buckling of unstiffened and stiffened VAT plates under uniform temperature change

Table 7: Maximum buckling temperature, ΔT_{cr} , for a square VAT laminated panel

Composites	(a) Unstiffened plate	Stiffened plate	
		(b) concentric stiffeners	(c) eccentric stiffeners
SF laminates	$50.60 (\pm \langle 45.00^\circ 45.00^\circ \rangle)$	$120.23, (\pm \langle 47.50^\circ 47.50^\circ \rangle)$	$347.25, (\pm \langle 60.00^\circ 60.00^\circ \rangle)$
VAT laminates	$57.15 (\pm \langle 62.50^\circ 35.00^\circ \rangle)$	$141.30, (\pm \langle 67.50^\circ 32.50^\circ \rangle)$	$383.87, (\pm \langle 65.00^\circ 50.00^\circ \rangle)$
Improvement	12.94%	17.52%	10.55%

buckling mode shapes corresponding to the maximum buckling temperature for each case are examined as shown in Fig. 13. The buckling mode shapes for the straight fiber (SF) and VAT laminated configurations obtained from the parametric studies for both unstiffened and stiffened plates are similar but not same as shown in Fig. 13. A large difference in the mode shapes for the plate with eccentric stiffeners is observed as shown in Figs. 13c. The in-plane stress resultants for both SF and VAT laminated configurations obtained from the parametric studies are studied as shown in Fig. 14. For symmetric laminates studied in this work, the in-plane shear stress resultant described in the global coordinate system, N_{xy} , is zero for all elements and hence they are not shown in the plot. It is found that for all cases, the VAT laminates cause a significant reduction in the stress resultant, N_{yy} , at the panel's center with a small increase in N_{xx} , as compared to that for the plate with SF laminates, resulting in an increase in the total buckling temperature.

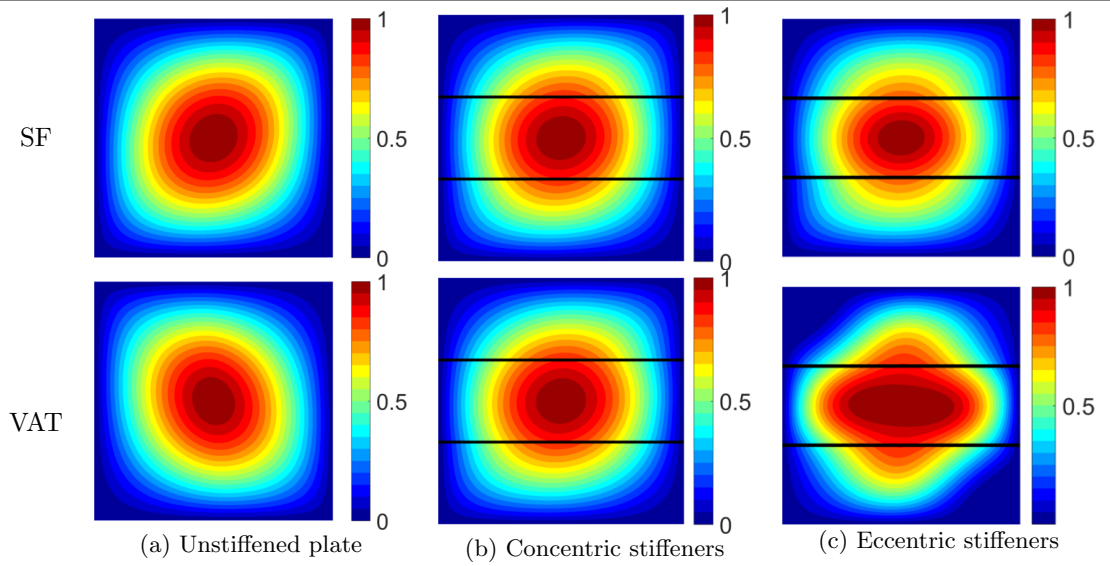
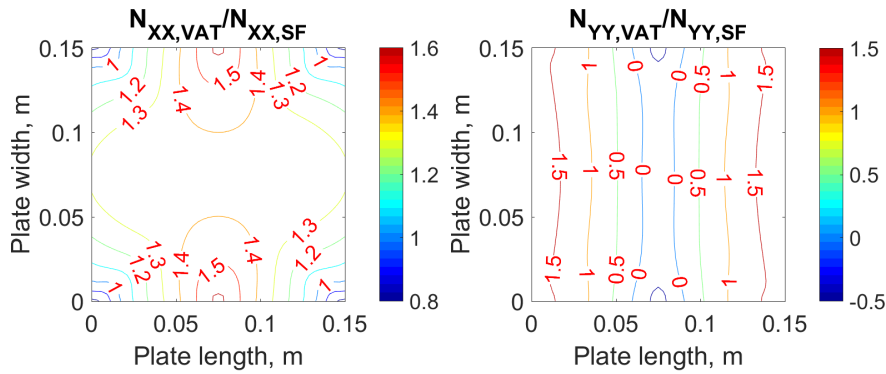
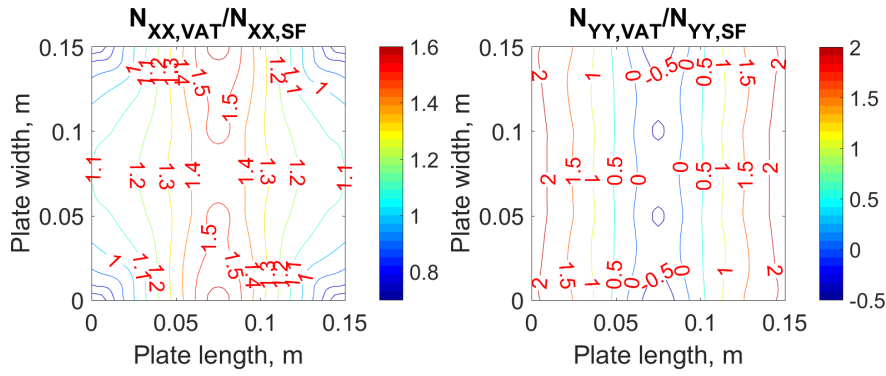


Figure 13: Buckling mode shapes corresponding to the maximum buckling temperature change

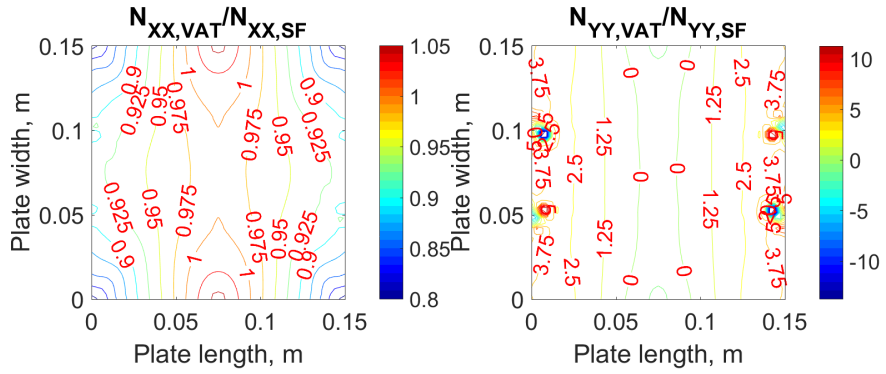
Previous research also show that the VAT laminates are mainly used to redistribute the in-plane stress resultant for improving the buckling load for the plate subjected to mechanical in-plane axial loads [25]. Recall that the curvilinear stiffeners can be used to tailor the buckling mode shape to increase the buckling load [49], it is possible to combine the use of curvilinear stiffeners and VAT laminates to improve the buckling response of a stiffened composite plate. In the following studies, concentric stiffeners for the curvilinearly stiffened VAT laminated plates are considered.



(a) Unstiffened plate



(b) Stiffened plate with two concentric stiffeners



(c) Stiffened plate with two eccentric stiffeners

Figure 14: In-plane stress resultant ratios of optimal VAT laminates over that with optimal SF laminates

C. Curvilinear Stiffeners

For a curvilinear stiffener, parameterized using the approach as presented in Section III, each stiffener has 4 shape design variables, along with two design variables for the fiber ply orientations, there are a total of 10 design variables for the stiffened VAT laminated plate with two stiffeners. It is very expensive to conduct a complete parametric study with respect to these 10 design variables. An optimization study is conducted to determine the optimal design in stiffener shape and laminate configuration. Before the optimization study, a simple parametric study is first conducted to investigate the influence of the stiffener shape on the buckling temperature of the plate. In fact, there are many stiffeners used for the plate to improve the buckling responses. Considering that the scope of the present paper is to study the effect of both curvilinear stiffeners and curvilinear fiber ply orientations on the structural buckling response, we only consider two curvilinear stiffeners in the parametric and optimization studies to reduce the computational burden, both in the CPU time and the required memory. Also, the size design variables, such as the geometric dimensions of the stiffener cross section, are not considered in the present study.

The start and end points for each curve are fixed in Fig. 15a. The middle control points have natural coordinates of $(0, \xi_2)$ and $(0, -\eta_2)$, respectively. The buckling temperature is studied by varying the parameter of η_2 from -1 to 1. The start and end points perimeter parameters for the curve ① are $\varepsilon_1^A = 0.1875$ and $\varepsilon_1^B = 0.6875$, respectively. The curve ② is symmetric to the curve ① about the panel center line, $y = b/2$. The VAT laminates of $(\pm[45^\circ] - 45^\circ)_2)_s$ is considered for the plate.

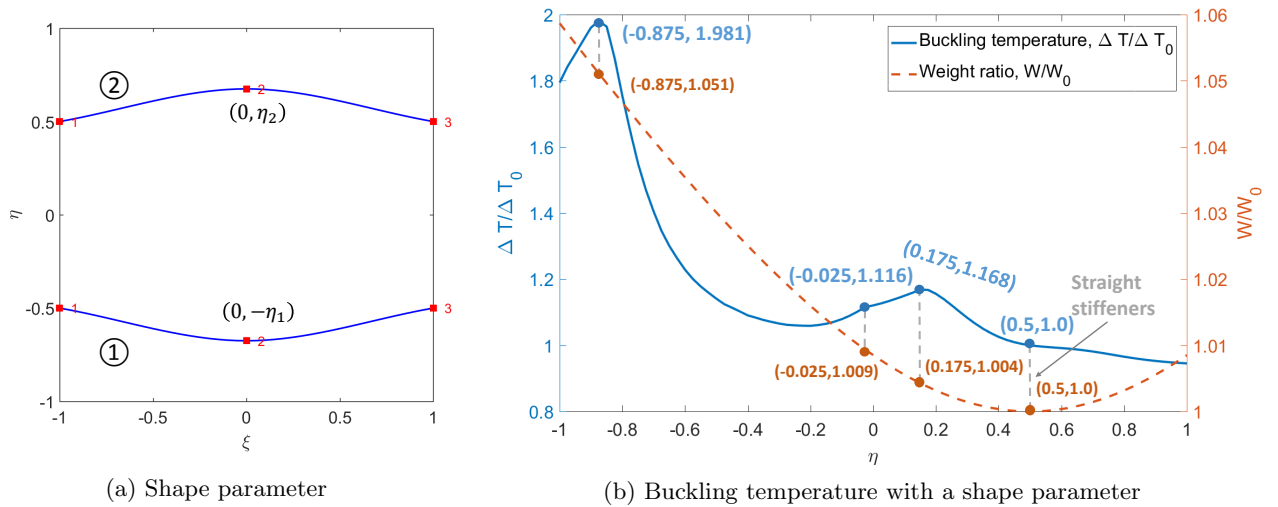


Figure 15: Buckling temperature varies with a shape parameter, η , for a curvilinearly stiffened VAT laminated plate

Figure 15b shows the buckling temperature and the total weight with the shape parameter, ξ_2 , in the

presence of a uniform temperature gradient. ΔT_0 and W_0 are buckling temperature and total weight for the panel with two straight stiffeners. As compared to the buckling responses for the plate with straight stiffeners, it is clearly observed that curvilinear stiffeners can improve the buckling temperature by up to 98.1% with weight penalty of 5.1% W_0 . There is also another stiffener shape where $\eta = 0.175$, leading an increase in the buckling temperature by 16.8% with merely 0.4% W_0 weight penalty.

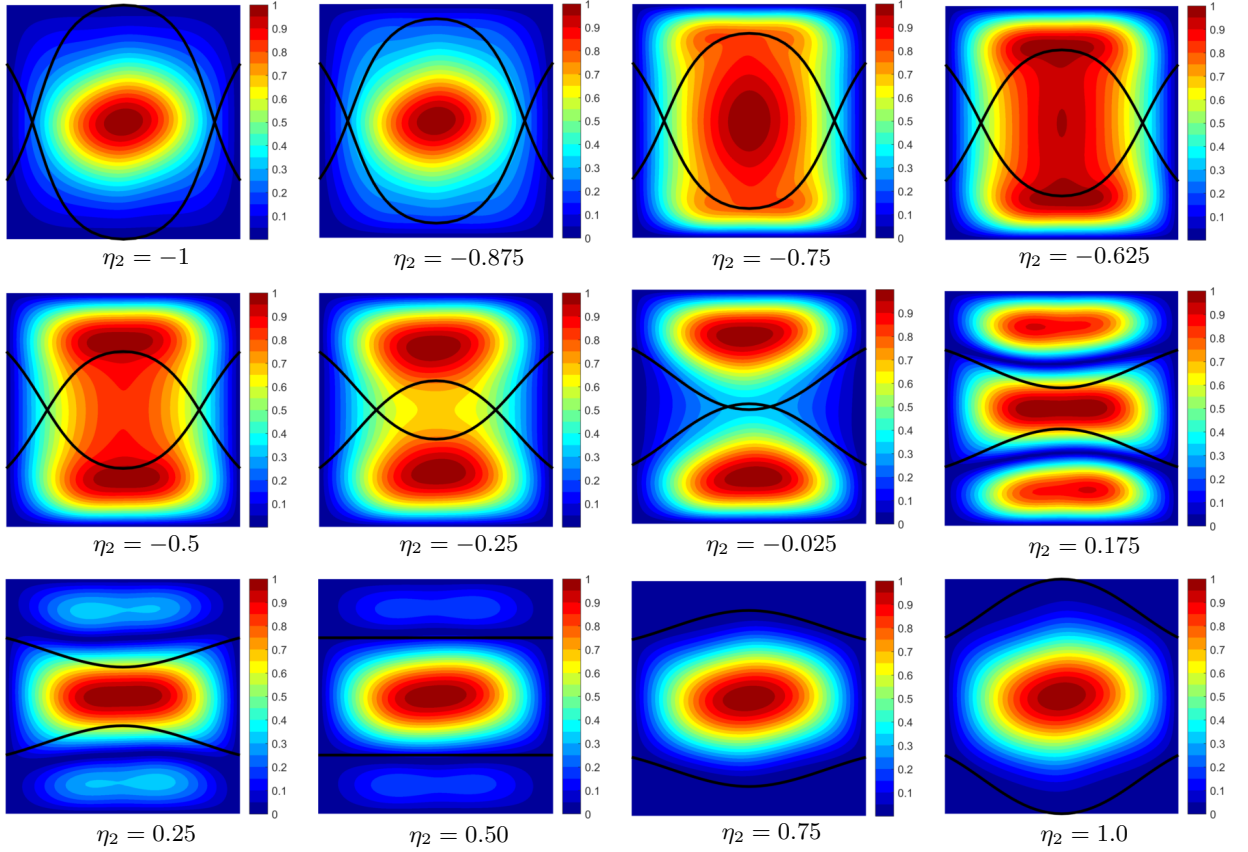


Figure 16: Thermal buckling mode shape for a stiffened plate with different shape parameters, η_2

The buckling temperature is found to change with the shape parameter in a discontinuous way. This is because the buckling mode shape changes with the shape parameter as seen in Fig. 16. It is clearly seen that the curvilinear stiffeners change the mode shape through modifying the buckling mode wavelength. This demonstrates that curvilinear stiffeners are used to tailor the buckling mode shape to increase the buckling temperature.

D. Thermal Buckling Optimization

Based on previous studies in Sections V-B and V-C, it is found that the VAT laminae can tailor the in-plane stress resultants for improving the buckling temperature for stiffened plate with fixed stiffeners. Also, the arbitrarily shaped stiffeners can modify the buckling mode wavelength for improving the buckling performance. This section combines using VAT laminates and curvilinear stiffeners together for improving the buckling temperature. Based on Fig. 12, it is seen that there are multiple peaks for the buckling temperature in terms of the fiber path angles. Therefore, the objective function in the optimization problem, buckling temperature, is not convex in terms of the fiber path angle and stiffener shape. It is easy to obtain local minima (buckling load multiplied by negative one) when using gradient based optimization. Previously developed particle swarm optimization (PSO) code with the parallel processing capability [44, 50] is used as the optimizer to maximize the buckling temperature for the stiffened plate with respect to both curvilinear stiffeners and VAT laminate fiber path angles. The optimization parameters used in PSO can be found in previous work[44, 50], which will not be shown here for brevity.

We conduct the buckling temperature maximization for the plate using VAT laminates and curvilinear stiffeners in a sequential way: (a) the straight fiber laminates and straight stiffeners (SF+SS), (b) the VAT laminates with linearly varying fiber path and straight stiffeners (VAT+SS) and (c) the VAT laminates and curvilinear stiffeners (VAT+CS). SF means straight fiber, SS means straight stiffeners and CS means curvilinear stiffeners. For all cases, the change in the stiffener shape leads to an increase in the total weight. The weight constraint for the stiffeners, W_s , is considered whose upper bound is the weight for the two straight x -axis stiffeners, $W_{s,0}$. The yielding strength and stiffener crippling constraints are not considered in this case, which will be added in future work. The optimization problem is summarized as:

$$\begin{aligned}
 & \text{maximize} && \Delta T_{b,cr} \\
 & \text{w.r.t.} && \{\Theta_0, \Theta_1, \varepsilon_{1,2}^A, \varepsilon_{1,2}^B, \xi_{1,2}^C, \eta_{1,2}^C\} \\
 & \text{s.t.} && W_s \leq W_{s,0} \\
 & && -90^\circ \leq \{\Theta_0, \Theta_1\} \leq 90^\circ \\
 & && 0 \leq \{\varepsilon_{1,2}^A, \varepsilon_{1,2}^B\} \leq 1 \\
 & && -1 \leq \{\xi_{1,2}^C, \eta_{1,2}^C\} \leq 1
 \end{aligned}$$

Since PSO is an evolutionary algorithm, which has stochastic characteristics [51], we have ran the optimization multiple times to get the best designs for all cases. The maximum buckling temperatures for all cases and their corresponding stiffener shape and the laminate configurations are shown in Table 8.

For all cases, the weight constraint is almost active. Because a numerical method is used in the present

Table 8: Optimal designs for the maximum buckling temperature

Composite Configuration	Laminates	Weight $W_s/W_{s,0}$	Buckling Temp. (°C)	Improvement ¹	Improvement ²
SF + Two Equi. stiffeners	$(\pm 47.50^\circ 47.50^\circ)$	1.00000	120.23	-	-
VAT + Two Equi. stiffeners	$(\pm 67.50^\circ 32.50^\circ)$	1.00000	141.30	17.52%	-
(a) SF + SS	$-\langle 45.02^\circ 45.02^\circ \rangle$	1.00099	140.14	15.56%	-
(b) VAT + SS	$-\langle 65.50^\circ 36.96^\circ \rangle$	1.00097	156.54	30.20%	11.70%
(c) VAT + CS	$-\langle 63.29^\circ 37.70^\circ \rangle$	1.00095	157.03	30.61%	12.05%

¹ improvement is computed with respect to the buckling temperature for case of SF + Two Equi. stiffeners

² improvement is computed with respect to the buckling temperature for case (a)

method, a slight violation criteria (0.001) in the weight is allowed. The optimal fiber path, optimal stiffener shape and the buckling mode shapes for each case are shown in Fig. 17. The buckling results for the optimal design cases are also verified using NASTRAN results. The present results are in a good agreement with NASTRAN results. Because a uniform temperature gradient is considered in this work, two stiffeners become almost perpendicular to each other for increasing the buckling temperature.

Table 8 shows that all optimal design cases can improve the buckling temperature when compared to that for the plate with two straight x -axis stiffeners by up to 30.6%. When compared to the buckling temperature for the plate using the optimal traditional design, *i.e.*, straight stiffeners and straight fiber laminates, the VAT laminates can further increase the buckling temperature for the plate by 11.7%. The optimal fiber paths in cases (b) and (c) are almost same. Also, the stiffener shapes for these two designs are almost similar. The slightly curved stiffeners and their placements for the case (c) change the buckling mode shapes, resulting in a 12.05% increase in the total buckling temperature. Based on the parametric studies given in Fig. 15b, curvilinear stiffeners can improve the buckling response but with a slight weight penalty. It is the weight constraint considered for the curvilinear stiffeners in the optimization study that limits the further improvement in the total buckling temperature. This motivates us to consider using an multiobjective optimization method for minimizing the weight and maximizing the buckling temperature for a stiffened plate with both VAT laminates and curvilinear stiffeners in future work.

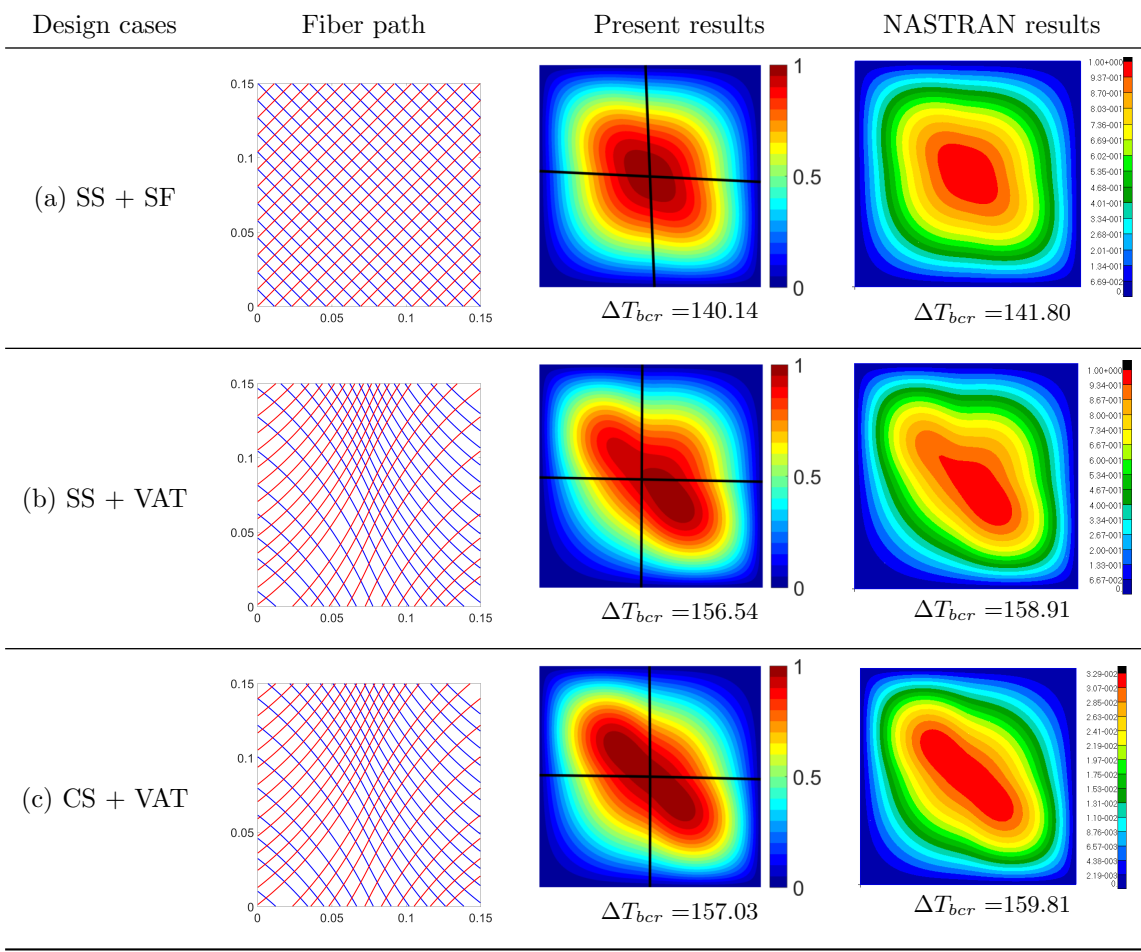


Figure 17: Optimal fiber plies for the first two layers, the optimal stiffener shape and the buckling mode shape

VI. Conclusion

This paper presents thermal buckling analysis and optimization of composite plates with both variable angle tow laminates and curvilinear stiffeners. A detailed derivation for computing the buckling temperature for the curvilinearly stiffened VAT laminates is presented. An innovative finite element approach is used for studying thermal buckling responses of the curvilinearly stiffened VAT laminates. This method obviates the requirement to place finite element nodes at the stiffener/plate and stiffener/stiffener interfaces when meshing such structures for structural analysis, which avoids the need for a relatively fine mesh for the stiffened plate having both spatially dependent fiber ply orientations and arbitrarily shaped stiffeners. Both elastic and geometric stiffness matrices for the beam elements that are used to model the stiffeners are transformed to those for the plate through the displacement compatibility conditions at the stiffener/plate interfaces

via finite element interpolation. Since all stiffeners are modeled using composite beam elements, and all the beam element nodal displacements are approximated using those for the plate, the displacement compatibility conditions at the stiffener/stiffener interfaces are satisfied automatically. Convergence and verification studies on the buckling temperatures for both unstiffened and stiffened laminated plates demonstrated the accuracy of the present method in thermal buckling analysis of curvilinearly stiffened VAT laminates.

Parametric studies on the buckling temperature for both unstiffened and stiffened plates, in terms of the fiber ply orientations, show that the VAT laminates can further improve the buckling responses for the plate as compared to that using straight fiber laminates by redistributing the in-plane stress resultants. The parametric study regarding the effect of the stiffener shape on the buckling temperature shows that the curvilinear stiffeners are able to tailor the buckling mode shape by modifying the buckling mode wavelength for improving the buckling response for the plate with a slight weight penalty.

Different optimization study cases using VAT laminates and arbitrarily shaped stiffeners are considered in a sequential way in the optimization study. Optimization results show that using VAT laminates and arbitrarily shaped straight stiffeners can increase the buckling temperature as compared to that using traditional design, *i.e.*, straight fiber laminates and straight stiffeners, with no weight penalty. The optimal design studied in this paper for the case of using curvilinear stiffeners and VAT laminates become almost same to that using straight stiffeners and VAT laminates in the presence of a uniform temperature gradient. However, the slightly curved stiffeners and their placements change the buckling mode shape resulting in a slightly higher buckling temperature. All of these results demonstrate that it is possible to use VAT laminates and arbitrarily shaped stiffeners together to further improve the thermal buckling for the plate as compared to the traditional design.

Appendix

A. The physical coordinates for the stiffeners ① and ② in Section V-A is:

$$\begin{aligned}x_1 &= [0.0000, 0.0168, 0.0290, 0.0440, 0.0559, 0.0703, 0.0813, 0.0939, 0.1033, 0.1125]; \\y_1 &= [0.0750, 0.0828, 0.0886, 0.0926, 0.1026, 0.1114, 0.1193, 0.1304, 0.1401, 0.1500] \\x_2 &= [0.0375, 0.0501, 0.0597, 0.0728, 0.0840, 0.0985, 0.1105, 0.1256, 0.1378, 0.1500]; \\y_2 &= [0.0000, 0.0136, 0.0231, 0.0338, 0.0414, 0.0499, 0.0561, 0.0635, 0.0693, 0.0750]\end{aligned}$$

References

- [1] Thornton, E. A., "Thermal Buckling of Plates and Shells," *Applied Mechanics Reviews*, Vol. 46, No. 10, 1993, pp. 485–506.
- [2] Collier, C., "Stiffness, Thermal Expansion, and Thermal Bending Formulation of Stiffened, Fiber-reinforced Composite panels," *34th Structures, Structural Dynamics and Materials Conference*, La Jolla, CA, pp. AIAA 1993-1569.
- [3] Biskner, A. and Higgins, J., "Design and Evaluation of a Reinforced Advanced-grid Stiffened Composite Structure," *46th AIAA/ASME/ASCE/AHS/ASC Structures, Structural Dynamics and Materials Conference*, Austin, Texas, AIAA 2005-2153.
- [4] Meetham, G. and de Voorde, M. H. V., "Materials for High Temperature Engineering Applications," Springer, 2000, pp. 127–139.
- [5] Gürdal, Z., Tatting, B. F., and Wu, K. C., "Tow-Placement Technology and Fabrication Issues for Laminated Composite Structures," *Proceedings of the 46th AIAA/ASME/ASCE/AHS/ASC Structures, Structural Dynamics and Materials Conference*, Austin, Texas, 2005, AIAA 2005-2017.
- [6] Gürdal, Z. and Olmedo, R., "In-plane Response of Laminates with Spatially Varying Fiber Orientations: Variable Stiffness Concept," *AIAA Journal*, Vol. 31, No. 4, 1993, pp. 751–758.
- [7] Forster, E., Clay, S., Holzwarth, R., Pratt, D., and Paul, D., "Flight Vehicle Composite Structures," *26th Congress of International Council of the Aeronautical Sciences (ICAS)*, Anchorage, Alaska, 2008, AIAA 2008-8976.
- [8] Velicki, A. and Thrash, P., "Advanced Structural Concept Development Using Stitched Composites," *49th AIAA/ASME/ASCE/AHS/ASC Structures, Structural Dynamics, and Materials Conference*, Schaumburg, IL, 2008, AIAA 2008-2329.
- [9] Lee, I., Lee, D.-M., and Oh, I.-K., "Supersonic Flutter Analysis of Stiffened Laminated Plates subject to Thermal Load," *Journal of Sound and Vibration*, Vol. 224, No. 1, 1999, pp. 49–67.
- [10] Chen, L.-W. and Chen, L.-Y., "Thermal Buckling Analysis of Composite Laminated Plates by the Finite-element Method," *Journal of Thermal Stresses*, Vol. 12, No. 1, 1989, pp. 41–56.

- [11] Meyers, C. A. and Hyer, M. W., "Thermal Buckling and Postbuckling of Symmetrically Laminated Composite Plates," *Journal of Thermal Stresses*, Vol. 14, No. 4, 1991, pp. 519–540.
- [12] Shiau, L.-C., Kuo, S.-Y., and Chen, C.-Y., "Thermal Buckling Behavior of Composite Laminated Plates," *Composite Structures*, Vol. 22, 2010, pp. 508–514.
- [13] Ounis, H., Tati, A., and Benchabane, A., "Thermal Buckling Behavior of Laminated Composite Plates: a Finite-element Study," *Frontiers of Mechanical Engineering*, Vol. 9, No. 1, 2014, pp. 41–49.
- [14] Reddy, J. N. and Chin, C. D., "Thermomechanical Analysis of Functionally Graded Cylinders and Plates," *Journal of Thermal Stresses*, Vol. 21, No. 6, 1998, pp. 593–626.
- [15] Zhao, X., Lee, Y., and Liew, K. M., "Mechanical and Thermal Buckling Analysis of Functionally Graded Plates," *Composite Structures*, Vol. 90, No. 2, 2009, pp. 161–171.
- [16] Duran, A., Fasanella, N., Sundararaghavan, V., and Waas, A., "Thermal Buckling of Composite Plates with Spatial Varying Fiber Orientations," *Composite Structures*, Vol. 124, 2015, pp. 228–235.
- [17] IJsselmuiden, S. T., Abdalla, M. M., and Gürdal, Z., "Thermomechanical Design Optimization of Variable Stiffness Composite Panels for Buckling," *Journal of Thermal Stresses*, Vol. 33, No. 10, 2010, pp. 977–992.
- [18] Gürdal, Z., Tatting, B. F., and Wu, C., "Variable Stiffness Composite Panels: Effects of Stiffness Variation on the In-Plane and Buckling Response," *Composites Part A: Applied Science and Manufacturing*, Vol. 39, No. 5, 2008, pp. 911–922.
- [19] Setoodeh, S., Abdalla, M. M., IJsselmuiden, S. T., and Gürdal, Z., "Design of Variable-Stiffness Composite Panels for Maximum Buckling Load," *Composite Structures*, Vol. 87, No. 1, 2009, pp. 109–117.
- [20] IJsselmuiden, S. T., Abdalla, M. M., and Gürdal, Z., "Optimization of Variable Stiffness Panels for Maximum Buckling Loads using Lamination Parameters," *AIAA Journal*, Vol. 48, No. 1, 2010, pp. 134–143.
- [21] Wu, Z., Weaver, P. M., Raju, G., and Kim, B. C., "Buckling Analysis and Optimisation of Variable Angle Tow Composite Plates," *Thin-walled Structures*, Vol. 60, 2012, pp. 163–172.
- [22] Coburn, B. H., Wu, Z., and Weaver, P. M., "Buckling Analysis of Stiffened Variable Angle Tow Panels," *Composite Structures*, Vol. 111, 2014, pp. 259–270.

- [23] Kapania, R. K., Li, J., and Kapoor, H., "Optimal Design of Unitized Panels with Curvilinear Stiffeners," *AIAA 5th ATIO and the AIAA 16th Lighter-than-Air Systems Technology Conference and Balloon Systems Conference*, 2005, AIAA 2005-7482.
- [24] Zhao, W. and Kapania, R. K., "Buckling Analysis of Unitized Curvilinearly Stiffened Composite Panels," *Composite Structures*, Vol. 135, 2016, pp. 365–382.
- [25] Zhao, W. and Kapania, R. K., "Prestressed Vibration of Stiffened Variable Angle Tow Laminated Plates," *AIAA Journal*, 2018, Under review.
- [26] Stanford, B. K. and Jutte, C. V., "Comparison of Curvilinear Stiffeners and Tow Steered Composites for Aeroelastic Tailoring of Aircraft Wings," *Computers and Structures*, Vol. 183, 2017, pp. 48–60.
- [27] Singh, K. and Kapania, R. K., "Optimal Design of Tow-Steered Composite Laminates with Curvilinear Stiffeners," *2018 AIAA/ASCE/AHS/ASC Structures, Structural Dynamics, and Materials Conference*, Kissimmee, FL, 2018, AIAA-2018-2243.
- [28] Mulani, S. B., Slemp, W. C., and Kapania, R. K., "EBF3PanelOpt: An Optimization Framework for Curvilinear Blade-stiffened Panels," *Thin-Walled Structures*, Vol. 63, 2013, pp. 13–26.
- [29] Jaunky, N., Knight Jr, N. F., and Ambur, D. R., "Formulation of an Improved Smeared Stiffener Theory for Buckling Analysis of Grid-Stiffened Composite Panels," *Composites Part B: Engineering*, Vol. 27, No. 5, 1996, pp. 519–526.
- [30] Nemeth, M. P., "A Treatise on Equivalent-Plate Stiffnesses for Stiffened Laminated-Composite Plates and Plate-Like Lattices," 2011, NASA TP-2011-216882.
- [31] Wang, D. and Abdalla, M. M., "Global and Local Buckling Analysis of Grid-stiffened Composite Panels," *Composite Structures*, Vol. 119, 2015, pp. 767 – 776.
- [32] Xu, Y., Tong, Y., Liu, M., and Suman, B., "A New Effective Smeared Stiffener Method for Global Buckling Analysis of Grid Stiffened Composite Panels," *Composite Structures*, Vol. 158, 2016, pp. 83 – 91.
- [33] Dähne, S. and Hühne, C., "Gradient Based Structural Optimization of a Stringer Stiffened Composite Wing Box with Variable Stringer Orientation," *World Congress of Structural and Multidisciplinary Optimisation*, Springer, 2017, pp. 814–826.

- [34] Caffrey, J. and Lee, J. M., *MSC/NASTRAN 2014 Linear Static Analysis: User's Guide*, 2014, MacNeal-Schwendler Corporation.
- [35] Leiva, H. S. V., *Structural Design Optimization of An Aircraft Composite Wing-box Using Curvilinear Stiffeners*, Fakultät Technik und Informatik, Department Fahrzeugtechnik und Flugzeugbau, 2014, Master's Thesis.
- [36] Singh, K., Zhao, W., Jrad, M., and Kapania, R. K., "Hybrid Optimization of Curvilinearly Stiffened Shells using Parallel Processing," *AIAA Journal of Aircraft*, 2018, In press.
- [37] Ahlbert, G., *Method Evaluation of Global-Local Finite Element Analysis*, Linköping University, 2012, Linkoping University, Department of Management and Engineering, Solid Mechanics, Master's Thesis.
- [38] Hobby, J. D., "Smooth, Easy to Compute Interpolating Splines," *Discrete and Computational Geometry*, Vol. 1, No. 2, 1986, pp. 123–140.
- [39] Honda, S., Narita, Y., and Sasaki, K., "Maximizing the Fundamental Frequency of Laminated Composite Plates with Optimally Shaped Curvilinear Fibers," *Journal of System Design and Dynamics*, Vol. 3, No. 6, 2009, pp. 867–876.
- [40] Hyer, M. W. and White, S. R., *Stress Analysis of Fiber-reinforced Composite Materials*, WCB McGraw-Hill, 1998.
- [41] Turvey, G. J. and Marshall, I. H., *Buckling and Postbuckling of Composite Plates*, Springer Science & Business Media, 2012.
- [42] Reddy, J. N., "Mechanics of Laminated Composite Plates: Theory and Analysis, Second Edition," CRC press, 2004, pp. 132–142.
- [43] Zhao, W. and Kapania, R. K., "Prestressed Vibration of Stiffened Variable Angle Tow Laminated Plates," *AIAA Journal*, 2018, Under review.
- [44] Zhao, W. and Kapania, R. K., "BLP Optimization of Composite Flying-wings with SpaRibs and Multiple Control Surfaces," *AIAA/ASCE/AHS/ASC Structures, Structural Dynamics, and Materials Conference, AIAA SciTech Forum*, Kissimmee, FL, 2018, AIAA 2018-2150.
- [45] Shi, Y., Lee, R. Y., and Mei, C., "Thermal Postbuckling of Composite Plates using the Finite Element Modal Coordinate Method," *Journal of Thermal Stresses*, Vol. 22, No. 6, 1999, pp. 595–614.

- [46] Walker, M., Reiss, T., Adali, S., and Verijenko, V. E., “Optimal Design of Symmetrically Laminated Plates for Maximum Buckling Temperature,” *Journal of Thermal Stresses*, Vol. 20, No. 1, 1997, pp. 21–33.
- [47] Zhao, W., Singh, K., and Kapania, R. K., “Thermo-mechanical Buckling of Curvilinearly Stiffened Variable Angle Tow Laminated Panels,” *22nd AIAA International Space Planes and Hypersonics Systems and Technologies Conference*, Orlando, FL, 2018, AIAA 2018-5156.
- [48] Timoshenko, S. P. and Gere, J. M., “Theory of Elastic Stability,” The McGraw-Hill Book Company, 1963, pp. 225–228.
- [49] Zhao, W. and Kapania, R. K., “Vibration Analysis of Curvilinearly Stiffened Composite Panels Subjected to In-plane loads,” *AIAA Journal*, Vol. 55, No. 3, 2017, pp. 981–997.
- [50] Liu, Q., Jrad, M., Mulani, S. B., and Kapania, R. K., “Global/Local Optimization of Aircraft Wing Using Parallel Processing,” *AIAA Journal*, Vol. 54, No. 11, 2016, pp. 3338–3348.
- [51] Eberhart, R. C. and Shi, Y., “Particle Swarm Optimization: Developments, Applications and Resources,” *Proceedings of the 2001 Congress on Evolutionary Computation*, Vol. 1, IEEE, 2001, pp. 81–86.